Metabolic Dysregulation and Adipose Tissue Fibrosis: Role of Collagen VI[∇][†]

Tayeba Khan,[1] Eric S. Muise,[2] Puneeth Iyengar,[1][‡] Zhao V. Wang,[3] Manisha Chandalia,[4]
Nicola Abate,[4] Bei B. Zhang,[5] Paolo Bonaldo,[6]
Streamson Chua,[7] and Philipp E. Scherer[3,8]*

Department of Cell Biology[1] and Department of Medicine,[7] Diabetes Research Center, Albert Einstein College of Medicine, Bronx, New York 10461; Departments of Molecular Profiling[2] and Metabolic Disorders,[5] Merck Research Laboratories, Rahway, New Jersey 07065; Departments of Internal Medicine[3] and Cell Biology,[8] Touchstone Diabetes Center, University of Texas Southwestern Medical Center, Dallas, Texas 75390-8549; Center for Human Nutrition, University of Texas Southwestern Medical Center, Dallas, Texas 75390[4]; and Department of Histology, Microbiology & Medical Biotechnologies, University of Padova, Viale Giuseppe Colombo 3, I-35121 Padua, Italy[6]

Received 15 August 2008/Returned for modification 29 October 2008/Accepted 22 December 2008

Adipocytes are embedded in a unique extracellular matrix whose main function is to provide mechanical support, in addition to participating in a variety of signaling events. During adipose tissue expansion, the extracellular matrix requires remodeling to accommodate adipocyte growth. Here, we demonstrate a general upregulation of several extracellular matrix components in adipose tissue in the diabetic state, therefore implicating "adipose tissue fibrosis" as a hallmark of metabolically challenged adipocytes. Collagen VI is a highly enriched extracellular matrix component of adipose tissue. The absence of collagen VI results in the uninhibited expansion of individual adipocytes and is paradoxically associated with substantial improvements in whole-body energy homeostasis, both with high-fat diet exposure and in the *ob/ob* background. Collectively, our data suggest that weakening the extracellular scaffold of adipocytes enables their stress-free expansion during states of positive energy balance, which is consequently associated with an improved inflammatory profile. Therefore, the disproportionate accumulation of extracellular matrix components in adipose tissue may not be merely an epiphenomenon of metabolically challenging conditions but may also directly contribute to a failure to expand adipose tissue mass during states of excess caloric intake.

Adipose tissue is a key regulator of systemic energy homeostasis. The physiological state of adipose tissue is driven by cell-autonomous processes within the adipocyte. In addition to this, the adipocyte itself is subject to major modifications by other cell types that infiltrate adipose tissue, such as macrophages and vascular cells; moreover, adipocytes can be markedly influenced by several hormones and cytokines that circulate systemically.

Although all these cellular interactions have been the subject of extensive studies in numerous laboratories, the extracellular matrix of adipose tissue has received limited attention to date, despite evidence suggesting that it is a functionally relevant constituent of adipose tissue physiology.

It is currently unknown what consequential effects metabolic stress exerts on the extracellular matrix and vice versa. In other words, what is the impact of dysregulation of the extracellular constituents of adipose tissue on the systemic metabolic state?

Here, we approach this subject from two different perspectives. We first assessed the overall level of extracellular matrix components under different metabolic conditions and established that the extracellular constituents are globally upregulated during metabolically challenging conditions. We then selected a specific member of the collagen family, collagen VI (exhibiting predominant expression in adipose tissue), and utilized a genetic model of collagen VI disruption to investigate the effects of disruption of the extracellular matrix of adipose tissue. Remarkably, our studies demonstrated that such weakening of adipose tissue extracellular matrix results in considerable improvement of the metabolic phenotype in the context of both a high-fat diet and a challenge with the *ob/ob* mutation.

Our observations highlight the extracellular matrix of adipose tissue as an important and novel site of modulation of systemic metabolism. Obese adipose tissue displays hallmarks similar to other fibrotic tissues, such as the liver; this suggests that specific constituents of this normally rather rigid extracellular matrix environment may provide possible targets for pharmacological intervention for the treatment of metabolic disorders.

MATERIALS AND METHODS

Animals. All animal experimental protocols were approved by the Institute for Animal Studies of the Albert Einstein College of Medicine or by the Institutional Animal Care and Use Committee of University of Texas Southwestern Medical Center at Dallas. Collagen VI-null mice were generated as previously described by Bonaldo and colleagues (4). The collagen VI-null *ob/ob* (*col6KOob/ob*) mice

were generated by mating heterozygous collagen VI-null mice (FVB background) with heterozygous leptin-deficient (*ob*/+) mice (C57 background). Mice were housed in groups of two to five in filter-top cages. The colony was maintained in a pathogen-free AALAC-accredited facility at the Albert Einstein College of Medicine under controlled environment settings (22 to 25°C; 40 to 50% humidity). Mice were maintained on a 12-hour light and dark cycle with ad libitum access to water and standard chow diet (no. 5058; Lab-Diet) or high-fat diet (no. D12492; Research Diets Inc.), as indicated. Experiments with the collagen VI-null mice were performed in a pure FVB background, while those with the *col6KOob/ob* mice were performed in a mixed C57/BL6 and FVB background. All experiments were littermate controlled. The majority of the experiments involving the *col6KOob/ob* mice were also independently reproduced in a pure FVB background.

Human subjects. This study was approved by the Institutional Review Board of UT Southwestern Medical Center (Dallas, TX). A written informed consent was obtained from every participant. Participants were recruited by public advertisements (fliers) placed in colleges, churches, temples, and South Asian grocery stores in the Dallas-Fort Worth metroplex. Height and weight were measured by standard procedures. A general health questionnaire was administered by trained technicians. Diabetes was excluded by measurement of fasting plasma glucose and glucose levels during a standard oral glucose tolerance test. Adipose tissue biopsy was obtained after overnight fasting, using a 14-gauge, 9-cm Temno II biopsy needle (Allegiance) to sample from subcutaneous abdominal and gluteal (peripheral) areas. Following skin preparation with betadine a small skin incision was made on the abdominal wall with a number 11 bladed scalpel. This facilitated guidance of the biopsy needle into the fat-containing subcutaneous space. Fat was collected from the abdominal wall in the right lower quadrant 2 cm above and medial to the anterior iliac tuberosity and from the gluteal area.

Oral glucose tolerance test and insulin tolerance test. For the oral glucose tolerance test, mice were fasted 2 h prior to administration of glucose (2.5 g/kg of body weight [BW]) by oral gavage. Tail venous blood was collected and assayed for glucose and insulin. Glucose was measured by an oxidase-peroxidase assay (Sigma-Aldrich) and insulin was measured with an insulin enzyme-linked immunosorbent assay kit (Millipore, Billerica, MA). Mice were denied access to food during the course of the study. For the insulin tolerance test, mice were fasted 2 h prior to administration of 1 U of human insulin (Novo Nordisk)/kg of BW by intraperitoneal injection. Tail venous blood was collected and assayed for glucose.

Triglyceride clearance. Mice were fasted for 2 h and given 15 μl of olive oil per gram of body weight by oral gavage. Approximately 20 μl of blood was collected at each time point and assayed for triglyceride (Infinity triglyceride kit; Thermo Electron Corp.) and free fatty acids (FFAs) (NEFA C; Wako). Mice were denied access to food during the course of the study.

LPS challenge. Ten-week-old male mice were injected intraperitoneally with lipopolysaccharide (LPS; Sigma-Aldrich) at a dose of 0.1 mg/kg of BW. For the LPS challenge time course, blood was collected at 0, 3, 6, and 24 h and assayed for interleukin-6 (IL-6) and monocyte chemoattractant protein 1 (MCP-1; R&D Systems), as indicated. For examination of adipose-specific inflammation in response to LPS, mice were sacrificed 90 min after LPS injection and tissues were immediately snap-frozen in liquid nitrogen.

PPARγ agonist gavage. The peroxisome proliferator-activated receptor gamma (PPARγ) agonist 2-(2-[4-phenoxy-2-propylphenoxy]ethyl) indole-5-acetic acid (COOH) was a kind gift from Merck Research Laboratories (Rahway, NJ). The COOH was given to 10-week-old male FVB mice by oral gavage daily at 12 noon for 14 days at a dose of 10 mg/kg BW. The mice were sacrificed 6 h after the last gavage and tissues were immediately snap-frozen in liquid nitrogen.

In vivo insulin signaling. Mice were fasted for 2 h and injected intraperitoneally with human insulin at a dose of 1 U/kg BW. Mice were sacrificed at 0, 5, or 10 min postinjection and tissues were immediately frozen in liquid nitrogen. Tissues were homogenized in radioimmunoprecipitation assay buffer supplemented with complete protease inhibitor cocktail and phosphatase inhibitor cocktail (Roche). The protein lysate was directly analyzed by Western blotting with anti-phospho-AKT (Cell Signaling Technology Inc.) and anti-Akt-1 (Santa Cruz Biotechnology Inc.). Western blot analysis was done using the Odyssey infrared imaging system (LI-COR Biotechnology).

Immunoblot analysis. Adipose tissues were homogenized in TNET buffer lacking Triton X-100 (150 mM NaCl, 5 mM EDTA, 50 mM Tris-HCl, pH 7.5) supplemented with complete protease inhibitor cocktail and phosphatase inhibitor cocktail (Roche). This was followed by low-speed centrifugation (3,000 × g at 4°C), in order to remove the fat cake from the top of the tube. Triton X-100 was added to the homogenate for a final concentration of 1% and the extract was cleared at 20,000 × g for 15 min at 4°C and mixed with 2× Laemmli sample

buffer. Protein samples were resolved on 4 to 12% bis-Tris gels, followed by transfer to BA83 nitrocellulose. Blots were probed with various antibodies, as indicated. Phospho-extracellular signal-regulated kinase (phospho-ERK), phospho-JNK, phospho-p38, ERK, and JNK antibodies were obtained from Santa Cruz Biotechnology; p38 antibody was obtained from Biosource; phospho-SMAD2, phospho-SMAD3, and total SMAD3 antibodies were obtained from Cell Signaling; total SMAD2 antibody was obtained from Invitrogen. Bound antibodies were detected with IRDye800-conjugated anti-rabbit or IRDye700-conjugated anti-mouse secondary antibodies (Rockland). Membranes were scanned with the LI-COR Odyssey infrared imaging system and band intensities were quantified with Odyssey v1.2 software (LI-COR Biotechnology).

Gene expression profiling. Animals were euthanized by CO_2 asphyxiation 6 h after the final dose (for drug treatments), and epididymal white adipose tissue was harvested and flash-frozen in liquid nitrogen. Total RNA was isolated after homogenizing the frozen tissues in TRIzol reagent (Invitrogen) with a PT10/35 Polytron (Kinematica AG) and processed using RNeasy kits (Qiagen) according to the manufacturers' instructions. RNA concentrations were estimated from the absorbance at 260 nm. Microarray processing was performed as previously described (24). Briefly, labeled cRNA was hybridized for 48 h onto Agilent 60-mer two-color spotted microarrays. Individual strain or compound treatment samples (including individual control or vehicle treatment samples) were hybridized against a control or vehicle treatment pool. The changes and *P* values were determined by averaging replicates (two to three replicates per strain or treatment) and using the Rosetta Resolver v6.0 software (Rosetta Inpharmatics LLC, a wholly owned subsidiary of Merck & Co., Inc., Seattle, WA). Change values represent the difference in regulation of the strain or compound-treated samples versus the control or vehicle-treated sample, and a positive value signifies upregulation following compound treatment or vice versa.

Quantitative real-time PCR analysis. Mice were sacrificed and tissue was immediately harvested and frozen in liquid nitrogen. RNA was extracted from tissue using TRIzol reagent (Invitrogen), followed by RNA isolation with the Qiagen RNeasy tissue kit. Total RNA (1 μg) was reverse transcribed with SuperScript III reverse transcriptase and oligo(dT)$_{20}$ (Invitrogen). Quantitative real-time PCR (qRT-PCR) was done using Sybr Green I master mix and was performed in the Roche Lightcycler 480. Primers were designed to span an intron in order to prevent amplification of any contaminating genomic DNA, if present. All PCRs were normalized to 18S rRNA, unless otherwise indicated, and relative expression levels were determined by the $\Delta\Delta C_t$ method with efficiencies of all primers being ~2 (35), which allowed us to make comparisons of relative abundance of the different collagens. The primer sets used are listed in Table S2 of the supplemental material.

Immunohistochemistry and staining procedures. Fresh adipose tissue was fixed in 10% phosphate-buffered formalin overnight. Paraffin wax sections of 5 μm were processed for immunostaining. For immunohistochemistry staining, sections were treated with peroxidase inactivation buffer for 10 min at room temperature to quench endogenous peroxidase activity (Dako) and incubated with primary antibodies for 24 h at 4°C. After washing, sections were incubated with biotinylated secondary antibodies for 1 h at room temperature, and the reaction was developed with ABC reagent (Vector Laboratories). All slides were counterstained with hematoxylin (Sigma-Aldrich). F4/80 staining was done with a rat monoclonal antibody (Invitrogen) and biotinylated rabbit anti-rat secondary antibody (Vector Laboratories). Additional staining methods included subcutaneous skin sections that were stained with Trichrome Masson stain and hematoxylin and eosin (H&E). Terminal deoxynucleotidyltransferase dUTP-biotin nick end labeling (TUNEL) staining was performed according to the manufacturer's protocol (Chemicon). All images were obtained with a Censys cooled charged-coupled-device camera (Photometrics, Tucson, AZ) on a Zeiss axiophot (Zeiss, Jena, Germany).

Quantitation of adipocyte size. Tissue sections from epididymal and mesenteric adipose tissue from 10-week-old mice were stained with H&E. Image J software was used to measure adipocyte area, which is represented as the average adipocyte area (in μm^2) or, alternatively, as the percentage of adipocytes in each 100-μm^2 area. Adipocyte size was measured from four mice/genotype (>500 cells/genotype).

Insulin/glucagon immunofluorescence staining and islet size quantification. Pancreas tissue was fixed in Bouin's fixative (saturated picric acid-formaldehyde-glacial acetic acid at a ratio of 15:5:1) for 5 h. Paraffin sections (5 μm) were incubated with control donkey immunoglobulin G (1:500; Jackson Immunoresearch Laboratories Inc.) for 1 h to block nonspecific binding. Sections were then incubated with guinea pig anti-mouse insulin antibody (1:500; a kind gift from Regina Kuliawat, Albert Einstein College of Medicine, Bronx, NY) and rabbit anti-human glucagon antibody (1:500; Invitrogen) overnight at 4°C. After washing three times with 1× phosphate-buffered saline, sections were incubated with

fluorescein isothiocyanate-conjugated donkey anti-guinea pig antibody and Texas Red-conjugated donkey anti-rabbit antibody (1:250; Jackson Immunoresearch Laboratories Inc.) for 1 h at room temperature. H&E-stained sections of the entire pancreas were cut so that the full face of the tissue was visible and were used for quantitation of islet size. Islets were visualized at 10× magnification; the islet area was measured with Image J and is expressed as the relative islet area/total area of the pancreas section, as described in reference 47. Sections were analyzed with an Olympus IX81 microscope.

TEM and SEM. For transmission electron microscopy (TEM), fresh adipose tissue was cut into 1-μm^2 pieces and fixed overnight in 2% paraformaldehyde, 2.5% glutaraldehyde in 0.1 M sodium cacodylate buffer. They were postfixed with 1% osmium tetroxide followed by 1% uranyl acetate, dehydrated through a graded series of ethanol, and embedded in LX112 resin (LADD Research Industries, Burlington, VT). Ultrathin sections (80 nm) were cut on a Reichert Ultracut UCT, stained with uranyl acetate followed by lead citrate, and viewed on a JEOL 1200EX transmission electron microscope at 80 kV. For scanning electron microscopy (SEM), fresh adipose tissue was cut into small blocks and analyzed as described in reference 7. Briefly, tissue was fixed overnight in 1:1 Karnovsky fixative, followed by the OTOTO method. The samples were dehydrated in a graded series of ethanol and infiltrated with hexamethyldisilazane. Samples were mounted on aluminum stubs and examined in a JEOL JSM6400 scanning electron microscope (Peabody, MA) using an accelerating voltage of 10 kV. False coloring was added to the images by using Adobe Photoshop.

Collagen content. Tissue collagen content was determined by staining formalin-fixed paraffin sections of epididymal adipose tissue in picro-sirius red (Sigma-Aldrich). Hydroxyproline measurement was done using a modified protocol of that described elsewhere (55). Briefly, 100 mg of frozen fat was heated in 6 N HCl at 110°C overnight in sealed tubes. The samples were then heated at 110°C for 48 h until dried. Each sample was incubated with chloramine-T (Sigma-Aldrich) at room temperature for exactly 20 min and then with p-dimethylaminobenzaldehyde (Fisher Scientific) at 60°C for 15 min. The absorbance was read at 540 nm and the concentration was determined by the standard curve created by cis-4-hydroxy-L-proline (Sigma-Aldrich).

Liver triglyceride measurements. Triglycerides were extracted from frozen liver tissues (200 mg) as described by Carr et al. (6a). Triglycerides were measured by a colorimetric assay using Infinity triglycerides (Thermo Scientific).

Body composition and indirect calorimetry measurements. Body composition was measured by magnetic resonance imaging (MRI) using an Echo MRI apparatus (Echo Medical Systems, Houston, TX). For indirect calorimetry measurements, animals were individually housed in metabolic chambers maintained at 20 to 22°C on a 12-h/12-h light-dark cycle with lights on at 0700. Metabolic measurements (oxygen consumption, respiratory exchange ratio, and locomotor activity) were obtained continuously using a CLAMS (Columbus Instruments, Columbus, OH) open circuit indirect calorimetry system. Mice were provided with the standard chow diet mentioned above and tap water ad libitum. Presented results contain data collected for a period of 8 days following 3 days of adaptation to the metabolic cages. For food intake measurements, mice were individually housed and food was weighed each day at noon for 7 days. Food intake is expressed as the grams of food ingested/gram of body weight.

Statistical analysis. Results are presented as means ± standard errors of the mean. Statistical analysis was performed with the Student t test or with a two-way analysis of variance (ANOVA) and subsequent Tukey test using GraphPad Prism 5 (San Diego, CA). Significance was accepted at a P value of <0.05.

RESULTS

Collagens are highly upregulated in adipose tissue during metabolic challenges. In order to assess the level of extracellular constituents under different metabolic conditions, we performed large-scale gene expression profiling on adipose tissue of several mouse models whose metabolic states vary over a vast range. A microarray comparison was performed on epididymal fat pads from db/db mice versus wild-type (WT) mice. In parallel, we compared WT mice treated with an antidiabetic PPARγ agonist (COOH) with vehicle-treated mice. We also extended the analysis to transgenic mice that constitutively overexpress adiponectin from adipocytes (adipoTG), a mouse model that we recently demonstrated to have an expanded fat mass with a metabolically healthy phenotype, mimicking

chronic exposure to PPARγ agonists (15, 28). Microarray results revealed that the vast majority of collagens are upregulated in adipose tissue from db/db mice (Fig. 1A). In contrast, mice treated with COOH or mice chronically overexpressing adiponectin display a downregulation of the collagens that are upregulated in the db/db state, suggesting that the majority of the extracellular matrix constituents are either direct or indirect targets for PPARγ. Since all conventional collagens (with the exception of collagen IX) behave surprisingly uniformly and are upregulated in the diabetic state, we believe the term "adipose tissue fibrosis" accurately describes the increased presence of extracellular matrix components during states of obesity and inflammation. This increased adipose tissue fibrosis may result in an increased rigidity of adipose tissue, potentially restricting further expansion of individual fat cells. To achieve a greater understanding of the relative abundance of the different collagens, we performed qRT-PCR on the conventional collagens I through VI (Fig. 1B) in a normal wild-type fat pad. Collagens I, IV, and VI were abundantly expressed in mature adipocytes, consistent with reports from other laboratories (39), while collagens II and III had considerably lower expression levels in adipocytes. Collagen VI was, however, the most predominant collagen in all fat depots examined.

Collagen VI expression is enriched in adipose tissue. In line with our original observations, we identified collagen VI alpha 3 (col6a3) as a major adipocyte-derived secretory protein (48) and subsequently demonstrated that the lack of adipose tissue-derived collagen significantly reduces tumor growth in the mammary gland (26). Collagen VI is distinct from its other collagen family members in that it is substantially enriched in adipose tissue (Fig. 1C). Results from these experiments confirmed the enrichment of collagen VI in adipose tissue, demonstrating high levels of expression in epididymal, mesenteric, subcutaneous, and perirenal fat pads, relative to the levels found in other tissues. Collagen VI may therefore have an important role in adipocyte physiology; consequently, collagen VI was selected for further in-depth analysis.

Gene expression profiling of epididymal fat from ob/ob and db/db mice demonstrated significantly increased levels of col6a3 during states of metabolic stress, with upregulation of 1.3-fold and 1.4-fold, respectively. In contrast, PPARγ agonist treatment of wild-type mice significantly reduced col6a3 levels by 1.6- to 1.9-fold (Fig. 1D, upper panel also see Table S1 in the supplemental material). Examination of several individual fat pads by qRT-PCR revealed that a 14-day PPARγ agonist treatment reduced levels of all three alpha-chains of collagen VI by 1.4- to 1.5-fold in epididymal fat (Fig. 1D, middle panel) and by 1.6- to 2.1-fold in mesenteric fat (Fig. 1D, lower panel).

In order to establish whether this phenomenon of increased collagen VI levels during periods of metabolic challenge is restricted to rodents or whether it is also relevant in the context of human disease, we examined col6a3 levels in a population of Asian Indian subjects and compared them to a matched control group of Caucasians. Despite similar body mass indices, the Asian Indian population has a higher level of susceptibility to insulin resistance than the Caucasian population (10). This is partly due to dysfunctional adipose tissue that tends to be more inflamed, even after adjustment for subcutaneous adipose tissue between Asian Indians and Caucasians (9). This
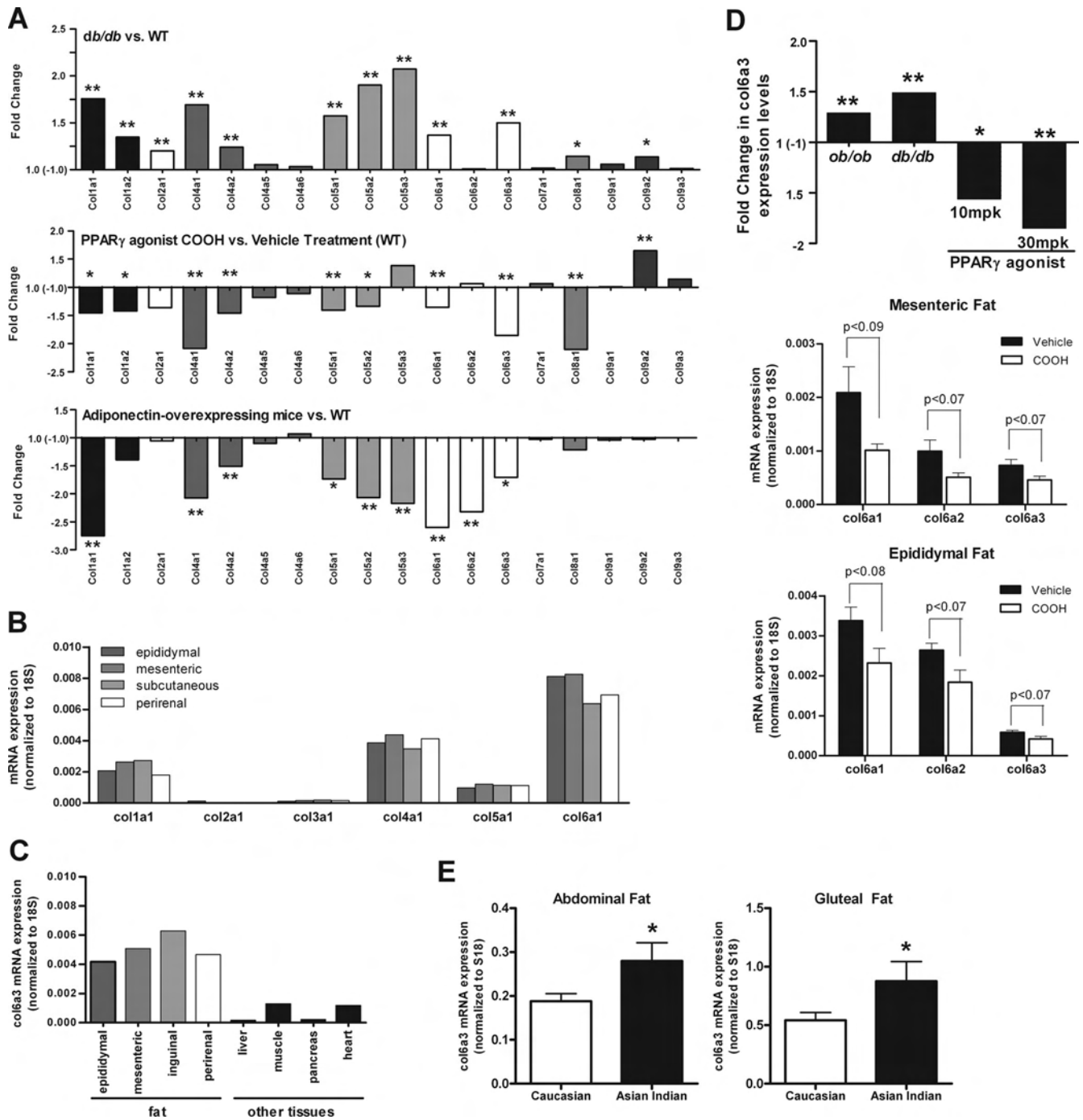
FIG. 1. Collagen VI expression levels correlate with different metabolic states. (A) Gene expression profiling of the major adipose tissue-expressed collagens in metabolically challenged mouse models was performed by microarray analysis. All microarray analyses were performed using epididymal fat. Results are expressed as the change in gene expression in *db/db* compared to WT mice (top graph), the change in WT mice treated with PPARγ agonist (30 mg/kg of COOH for 7 days) compared to WT mice treated with vehicle (middle graph), and the change in adiponectin-overexpressing mice compared to WT mice (bottom graph). Labeled cRNA from each individual experimental strain and treatment ($n \geq$ three mice) was competitively hybridized against a cRNA pool from the respective control group ($n \geq$ three mice) onto Agilent microarrays. A positive change is indicative of an upregulation in the experimental strain or treatment group, and vice versa. (B) Collagen VI is the predominantly expressed collagen in fat. The major adipose tissue-expressed collagens (collagen I, II, III, IV, V, and VI) were measured in epididymal, mesenteric, inguinal, and perirenal fat pads by qRT-RCR in 8-week old WT mice ($n = 2$). Expression levels were normalized to 18S rRNA. A representative example is shown. (C) Collagen VI expression is enriched in adipose tissue. Collagen VI alpha 3 levels were measured by qRT-PCR in the major fat pads and other tissues of 8-week-old WT mice ($n = 2$). Expression levels were normalized to 18S rRNA. A representative example is shown. (D) Collagen VI alpha 3 expression levels positively correlate to metabolically challenged states. Expression levels were determined by using Agilent microarrays, as described for panel A. Results show the change in collagen VI alpha 3 expression levels in *ob/ob* and *db/db* mice versus WT mice and the change in WT mice treated with 10 or 30 mg/kg (mpk) PPARγ agonist versus vehicle treatment (upper panel) ($n \geq$ three mice/group, except for the 10-mg/kg PPARγ agonist treatment, which included two mice). Collagen VI expression
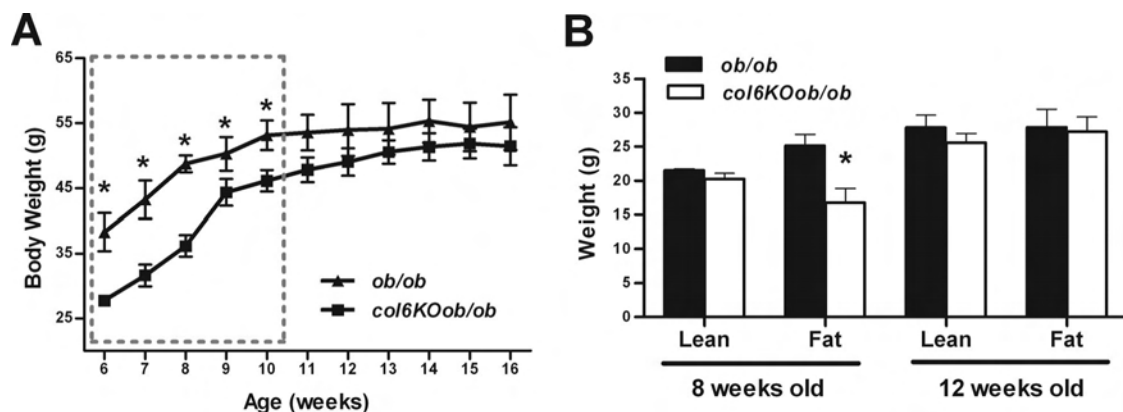
FIG. 2. *col6KOob/ob* mice have reduced body weights due to a decrease in fat mass at a young age. (A) Body weight was monitored for a period of 10 weeks (mean $\pm$ standard error; n = four mice/group). (B) Body compositions of 8-week-old and 12-week-old mice were determined by magnetic resonance imaging using an ECHO MRI (mean $\pm$ standard error; n = four mice/group). *, $P < 0.05$. (A) Data were analyzed by two-way ANOVA; (B) data were analyzed by Student's *t* test.

therefore represented a unique opportunity to dissociate obesity from metabolic dysfunction. Consistent with the observations in the metabolically challenged preclinical models, *col6a3* expression was significantly increased in both the abdominal and gluteal subcutaneous adipose depots in this Asian Indian cohort (Fig. 1E). This suggests that the upregulation of collagen VI is also a hallmark of dysregulated human adipose tissue.

ob/ob mice lacking collagen VI have lower body weights at an early age. In order to explore whether increased rigidity of the extracellular matrix merely correlates with a metabolically challenged state or whether it is a driving force with a direct functional impact on adipose tissue, we examined the metabolic consequences of a destabilized extracellular matrix in a genetic mouse model. Collagen VI is a heterotrimer, assembled from three alpha chains: alpha 1, alpha 2, and alpha 3. As previously described (4), the disruption of collagen VI alpha 1 leads to an overall functional null phenotype for collagen VI, since in the absence of the alpha 1 chain, the alpha 2 and 3 chains cannot be secreted effectively. This results in the absence of any collagen VI deposition in the extracellular matrix. We exposed collagen VI-null (*col6KO*) mice to a strong metabolic challenge by breeding these null mice into the *ob/ob* background. Analysis of age-dependent weight gain revealed that *col6KOob/ob* mice had lower body weights at an early age and remained lighter until about 11 weeks of age. After this point, the body weights of *col6KOob/ob* mice caught up to their *ob/ob* littermates and their weights were no longer statistically different (Fig. 2A). Body composition analysis by echo MRI indicated that the weight differences observed at a younger age

were primarily due to differences in fat mass, whereas older animals had a body composition comparable to *ob/ob* mice (Fig. 2B).

Lack of collagen VI improves the metabolic phenotype in ob/ob mice. Several metabolic parameters were measured in the *col6KOob/ob* mice. Fasting glucose levels in 10-week-old *col6KOob/ob* were normalized (Fig. 3A). When challenged with an oral glucose tolerance test, *col6KOob/ob* mice showed dramatically improved glucose clearance for the duration of the challenge. Comparable metabolic improvements were also found in 12-week-old mice, at which time there were no longer differences in adiposity (Fig. 3B). Similar trends were observed if the *col6KO* mice without the *ob/ob* mutation were subjected to a high-fat diet. The lack of collagen VI leads to reduced weight gain (Fig. 3C), due to reduced fat accumulation (a representative picture of the subcutaneous and intradermal fat layers is shown in Fig. 3D), with improvements in glucose clearance during an oral glucose tolerance test (data not shown). Since the phenotype obtained from high-fat diet exposure and the phenotype of *col6KO* mice crossed into the *ob/ob* background were nearly identical, we performed the remaining metabolic characterizations utilizing mice carrying the *ob/ob* mutation.

***col6KOob/ob* mice have improvements in lipid clearance.** Additional improvements of the *col6KOob/ob* mice were observed during an oral triglyceride challenge. In contrast to the reduced lipid clearance rate that is typically observed in *ob/ob* mice, the *col6KOob/ob* mice had an increased rate of triglyceride disposal (Fig. 3E, left). However, there was no significant change in serum FFA during this lipid challenge (Fig. 3E,

was reduced in adipose tissue by PPARγ treatment (middle and lower panels). Wild-type mice (10 weeks old) were treated with 30 mg/kg COOH or vehicle for 14 days by oral gavage. Collagen VI alpha 1, alpha 2, and alpha 3 mRNA levels were measured in epididymal (middle panel) and mesenteric (lower panel) fat by qRT-PCR and were normalized to 18S rRNA (mean $\pm$ standard error; n = four mice/group). (E) Collagen VI expression is increased in metabolically obese individuals. Collagen VI alpha 3 levels were measured in subcutaneous abdominal and gluteal (peripheral) adipose tissue in Asian Indians (18 men and 4 women), a metabolically obese group, and compared to control Caucasian populations of similar ages (27 ± 4 and 28 ± 7 years, respectively) and body mass indices (24 ± 4 and 25 ± 6 kg/m^2, respectively). Expression levels were measured by qRT-PCR and normalized to 18S rRNA (means $\pm$ standard errors; n = 15 to 19 Caucasians, n = 24 to 30 Asians). *, $P < 0.05$; **, $P < 0.01$ by Student's *t* test.
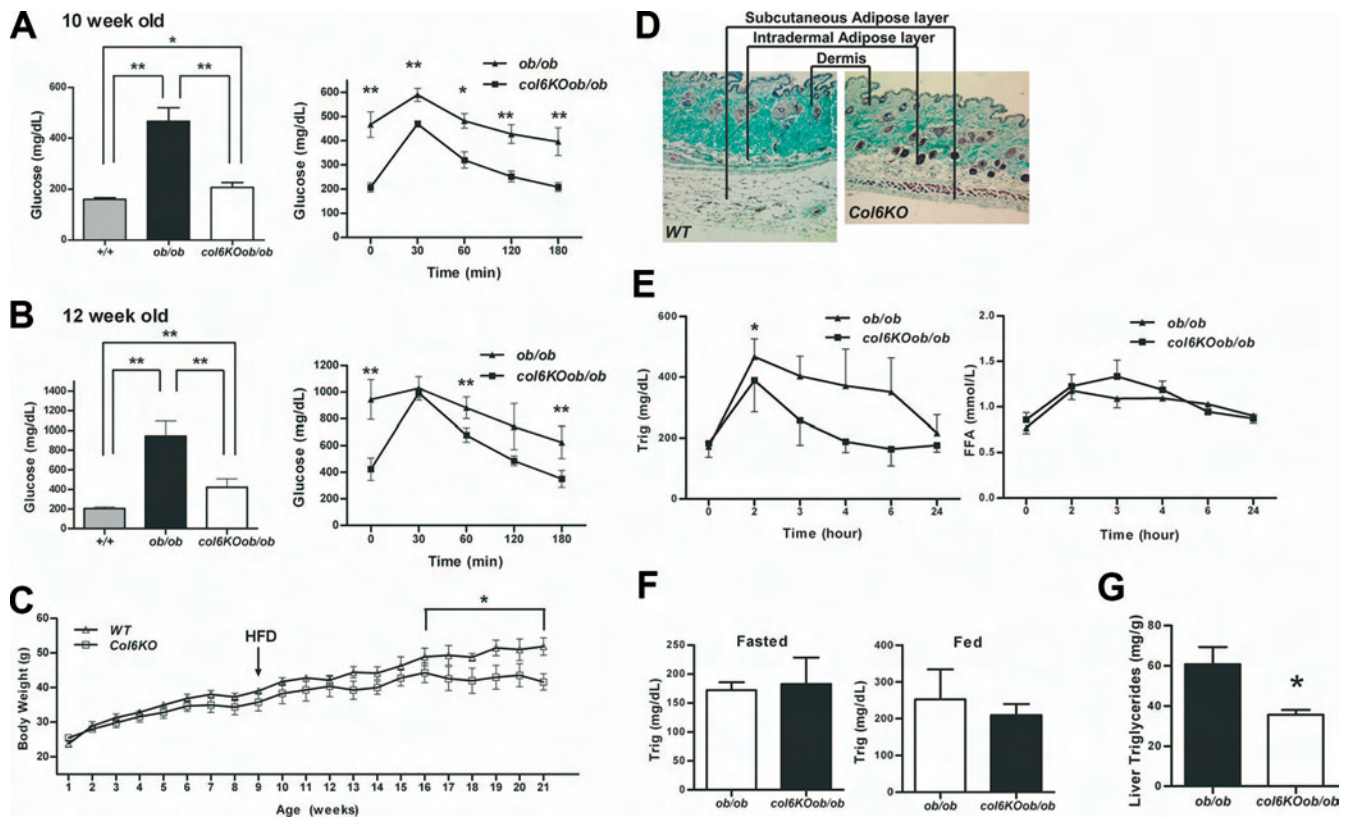
FIG. 3. The absence of collagen VI normalizes the metabolic profile of *ob/ob* mice and mice receiving a high-fat diet challenge. (A and B) Fasting glucose (left) and circulating glucose levels during an oral glucose tolerance test (right) in 10-week-old (A) and 12-week-old (B) *col6KOob/ob* and *ob/ob* mice. (C) Body weight was monitored in collagen VI-null and wild-type littermates. A 12-week high-fat diet challenge was initiated at week 9. In panels A to C, data are represented as means ± standard errors (*n* = four mice/group). (D) Trichrome Masson stain of subcutaneous skin sections from collagen VI-null and WT mice after a 12-week high-fat diet (HFD) challenge. (E) Circulating triglycerides (Trig) (left panel) and FFA (right panel) were measured during a lipid challenge in 10-week-old *col6KOob/ob* mice (mean ± SE; *n* = four mice/group). (F) Fed and fasted triglyceride levels in 10-week-old *col6KOob/ob* mice. (G) Liver triglyceride content was measured by chloroform-methanol extraction and a colorimetric assay (as described in Materials and Methods) (means ± standard errors; *n* = four mice/group). (H) H&E-stained pancreatic sections from 10-week-old male mice revealed reduced islet hyperplasia in *col6KOob/ob* mice compared to *ob/ob* littermates (upper panel). Sections of the full face of the pancreas were used to quantitate islet area. Islet area was determined at 10× magnification and is expressed as the islet area (μm²)/area of entire pancreas section (μm²) (means ± standard errors; *n* = five mice/group). Immunofluorescence staining of pancreas sections for insulin (green) and glucagon (red) showed improved α and β cell distributions in *col6KOob/ob* mice (lower panel). (I) Transmission electron microscopy of epididymal adipose tissue from 16-week-old *col6KOob/ob* and *ob/ob* mice. The arrow specifies a representative invaginated caveolae, while the arrowhead specifies an uninvaginated caveolae. The doubleheaded arrow indicates the interstitial space between two adipocytes. (J) Insulin signaling in 10-week-old *col6KOob/ob* mice and their *ob/ob* littermates that were injected with 1 U insulin/kg BW and from whom epididymal adipose tissue was collected 0, 5, and 10 min postinjection. The phosphorylation state of AKT was determined by Western blotting directly with specific antibodies for P-AKT and total AKT levels. Band intensities were quantitated with the LI-COR imaging system (LI-COR Biosciences) (means ± standard errors; *n* = three mice/group). ∗, $P < 0.05$; ∗∗, $P < 0.01$ (by Student's *t* test or by two-way ANOVA).

right). Fasted and fed triglyceride levels were unchanged in the *col6KOob/ob* mice (Fig. 3F). *col6KOob/ob* mice also displayed a significant reduction in the degree of lipid accumulation in the liver. The *ob/ob* mice accumulated characteristically high levels of hepatic triglycerides (Fig. 3G), whereas the levels of hepatic lipids in the *col6KOob/ob* mice were significantly improved. These results suggest that in the absence of collagen VI, mice not only display improvements in carbohydrate metabolism but also exhibit significant improvements in lipid metabolism.

Lack of collagen VI improves the pancreatic hyperplasia typical of *ob/ob* mice. In view of the many improvements in carbohydrate and lipid metabolism in the absence of collagen VI, the question arises as to whether these improvements could further manifest at the level of the pancreas. We histo-

logically examined pancreatic islets, with an emphasis on β cells. A significant improvement in pancreatic islet morphology could indeed be observed in *col6KOob/ob* mice. H&E staining of the pancreas revealed the expected β cell hyperplasia characteristic of *ob/ob* islets relative to wild-type islets, prompted by the high degree of insulin resistance (Fig. 3H, upper panel). Lack of collagen VI resulted in a reduction of islet area. This was also apparent after a more quantitative assessment. Immunofluorescent analysis of islets was performed to further underline improvements in overall islet architecture by staining for α (red) and β (green) cells to highlight the number and distribution of these two cell types within the islets (Fig. 3H, lower panel). Islets from *col6KOob/ob* mice have an α/β cell distribution similar to wild-type mice, with the expected distri-
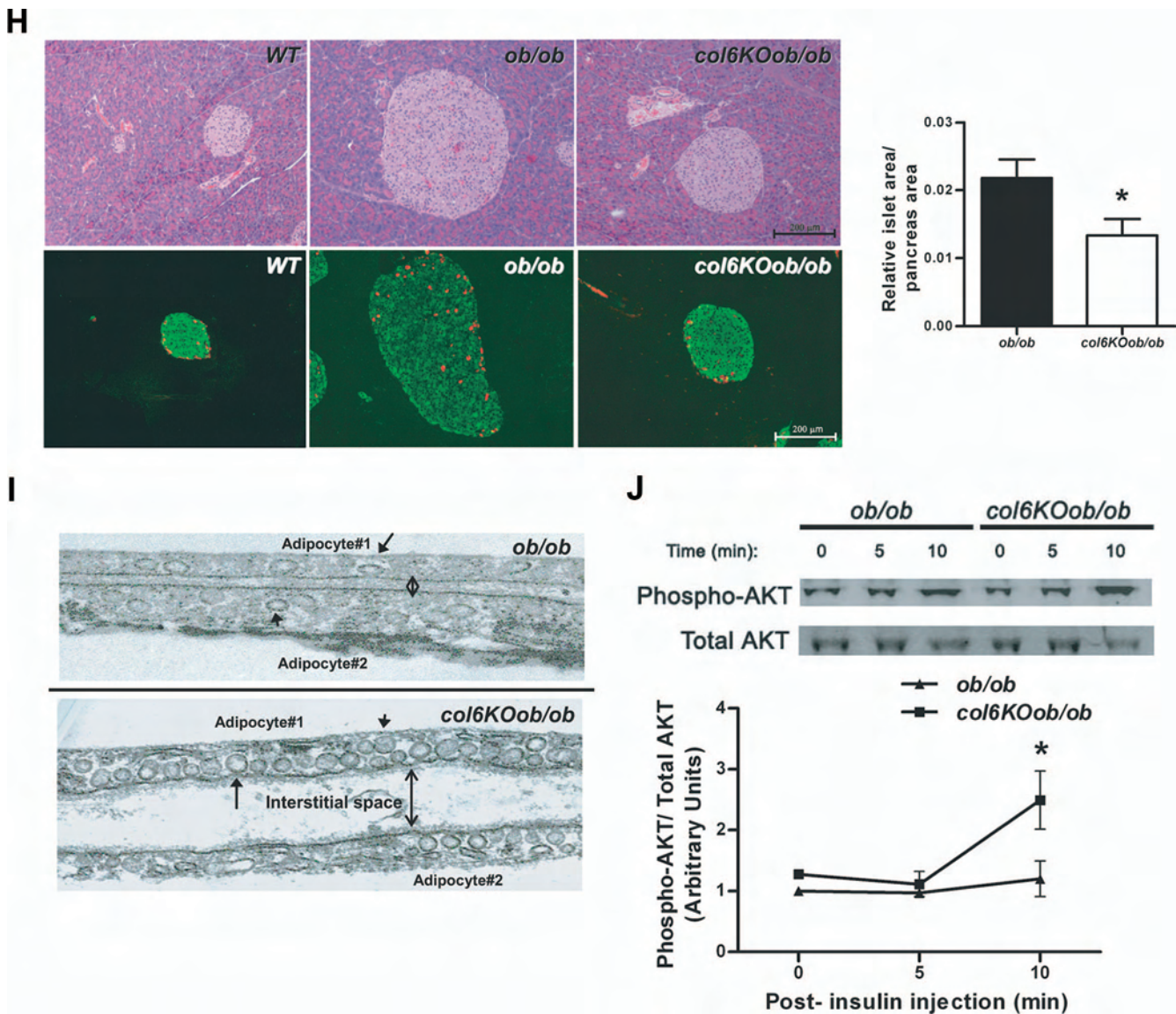
FIG. 3—Continued.

bution of α cells on the outer edge of the islets and the β cells in the center of the islets, as opposed to the more disorganized overall architecture in the *ob/ob* islets. A direct, quantitative comparison of islet area per pancreas area between the *ob/ob* and *col6KOob/ob* islets highlighted the overall smaller islets in mice lacking collagen VI. Therefore, the overall size and morphology of the islets in *col6KOob/ob* mice showed significant improvements.

***col6KOob/ob* mice have an increased number of plasma membrane caveolae and altered insulin signaling in adipose tissue.** Lipid rafts/caveolae play a major role in insulin signaling in the adipocyte through stabilization of the insulin receptor (14). Visual inspection of numerous adipocytes by TEM suggests that plasma membranes of *col6KOob/ob* and *col6KO* adipocytes display dramatic ultrastructural alterations. *col6KOob/ob* mice have a dramatically increased number of caveolae and an increased interstitial space between adipo-

cytes relative to *ob/ob* mice (Fig. 3I). While many of these caveolar invaginations of the plasma membrane have the typical flask-shaped conformation, there are a substantial number of caveolar structures that appear to be unattached from the plasma membrane in the *col6KOob/ob* adipocytes. In contrast, *ob/ob* mice have a more conventional caveolae arrangement, thus making it apparent that changes in the composition of the extracellular matrix translate into changes in caveolar invagination with the plasma membrane. It is known that caveolae play important roles in adipocyte function. One well-described phenomenon is the association of caveolin-1, a key structural and regulatory component of caveolae, with the insulin receptor. We therefore considered whether the altered state of caveolar structures in *col6KOob/ob* adipocytes alters local insulin sensitivity in adipose tissue. As suggested by the increased caveolae density in adipocytes, *col6KOob/ob* mice have increased AKT activation upon insulin stimulation in adipose
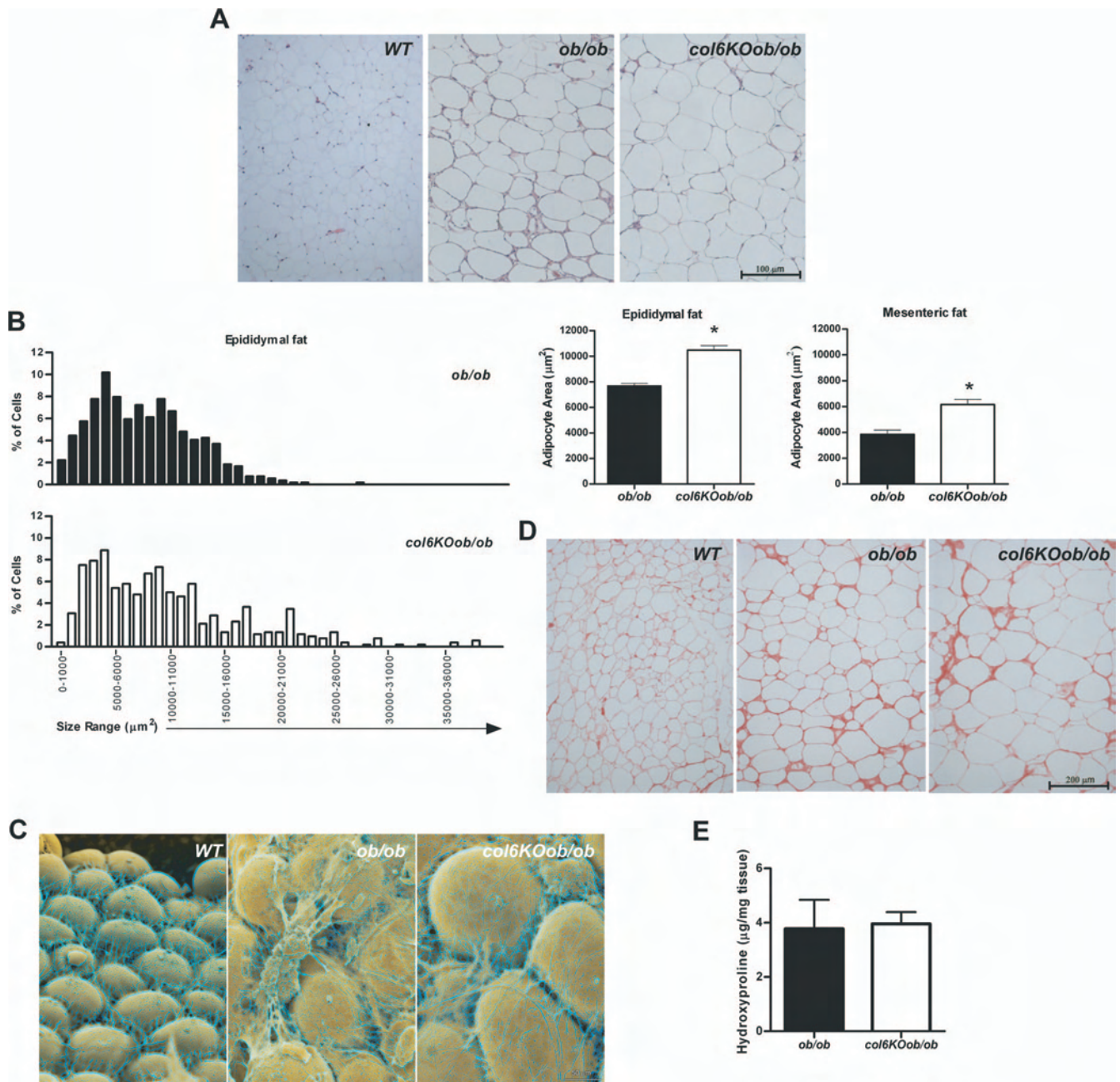
FIG. 4. *col6KOob/ob* mice have larger adipocytes. (A) H&E-stained tissue sections of epididymal adipose tissue from *col6KOob/ob* mice and their *ob/ob* littermates. (B) The adipocyte area was calculated from epididymal and mesenteric adipose tissue sections using ImageJ software. The graph on the left shows the percentage of adipocytes in every 100-μm^2 area range. Average adipocyte areas in epididymal and mesenteric fat are shown in the right panel. Adipocyte area was determined from four mice/group (>500 cells counted/group). *, $P < 0.05$ by Student's *t* test. (C) False-colored scanning electron micrographs of adipocytes from epididymal adipose tissue. (D) Sirius red staining of collagen from epididymal fat. (E) Hydroxyproline content of epididymal fat was measured as an indicator of total collagen content. All experiments (A to E) were performed on 8-week-old mice.

tissue (Fig. 3J). After 10 min of insulin stimulation, AKT phosphorylation is twofold higher in *col6KOob/ob* mice than in *ob/ob* littermates, indicating improvements in insulin signaling.

Collagen VI-null mice have an increased adipocyte cell size. Metabolic improvements are generally associated with a reduction in average fat mass and cell size. Histological examination of epididymal (Fig. 4A) and mesenteric (data not shown)

adipose tissues revealed that adipocytes are bigger in *col6KOob/ob* fat compared to adipocytes from their *ob/ob* littermates. This is surprising, since average adipocyte cell size in *ob/ob* mice is already drastically increased relative to wild-type adipocytes. This propensity toward larger adipocytes is not unique to *col6KO* mice in the *ob/ob* background but can also be seen in *col6KO* mice on a high-fat diet (data not shown). A

quantitative assessment of the adipocyte size distribution clearly underlines this shift toward larger adipocyte areas in the collagen VI-null model (Fig. 4B). In view of the overall metabolic improvements in the *col6KOob/ob* mice, this increase in cell size is quite unexpected, since improvements in metabolism are generally associated with smaller adipocytes rather than larger adipocytes. Visualization of the adipocytes by scanning electron microscopy confirmed the larger adipocyte size but also depicted a less restrictive adipocyte environment through an altered extracellular matrix composition (Fig. 4C). Collagen VI clearly constitutes an important component of the extracellular matrix environment in adipose tissue. Lack of collagen VI results in a less dense and less structured adipose tissue. This led us to speculate that this change in texture is due to changes in the overall collagen content of the tissue. Two independent methods were utilized to assess total collagen content in the extracellular matrix of the *col6KOob/ob* mice. A Sirius connective tissue stain was performed on the adipose tissue, which did not reveal any major histological differences (Fig. 4D). As a more quantitative measure of assessment, hydroxyproline content of the tissue was also determined. Since hydroxyprolines are a major component of collagens, quantification of levels of this modified amino acid is considered an accurate indicator of overall collagen content. Despite the less structured, visually apparent structural changes in the *col6KOob/ob* fat, these two methods confirmed that overall collagen content was not altered (Fig. 4E). This may be due to an induction of other collagens in the absence of collagen VI. More likely, this is due to the fact that collagen VI contains only relatively minor stretches of classical collagen repeats that are hydroxyprolinated and it will therefore not have a significant impact on total tissue hydroxyproline. Nevertheless, collagen VI makes a unique contribution to the stability of the extracellular matrix environment in adipose tissue.

We were interested in determining if the obese state could be considered as a state of fibrosis and whether the loss of collagen VI could reduce this level of fibrosis. Therefore, we examined the levels of several genes with well-established roles in fibrosis and found that the levels of many key fibrotic genes are altered. Lumican and decorin are proteoglycans that have been previously identified to bind fibrillar collagens, including collagen VI (3, 21, 52), and can interfere with collagen fibrillogenesis (40, 45). These genes have a major involvement in the epithelial-mesenchyme transition that occurs during fibrosis, a process during which epithelial cells differentiate and take on a more mesenchyme-like morphology (30, 46). Lumican has stimulatory effect on the epithelial-mesenchymal transition state of fibrosis, while in contrast decorin has an inhibitory role in transforming growth factor β (TGF-β)-induced fibrosis (30, 45). Quantitative real-time PCR revealed that mRNA levels of lumican were downregulated, while decorin levels were upregulated. TGF-β levels were also downregulated in *col6KOob/ob* adipose tissue (Fig. 5A). Upon further examination of lumican and decorin levels during various metabolic states, we found that lumican levels positively correlated with obesity (*ob/ob* and *db/db*) and negatively with an improved metabolic state (PPARγ agonist treatment or adipoTG mice) (Fig. 5B). Similarly, TGF-β was also regulated by PPARγ agonist treatment (Fig. 5C). This suggests that lumican and TGF-β play a critical role in regulating fibrosis during obe-

sity. This can be confirmed at the protein level, where TGF-β protein levels are reduced. This also results in decreased activation of downstream TGF-β signaling mediators, such as SMAD2 and SMAD3, whose phosphorylation state was also reduced (Fig. 5D).

Interestingly, the absence of collagen VI also resulted in reduced levels of elastin (Fig. 5A), a key molecule in matrix elasticity whose main function is to return cells to their original shape upon stretching. This reduced force on *col6KOob/ob* adipocytes to retract to their original shape suggests that the adipocytes are able to stretch and expand with less tension from the elastin fibers, which would typically attempt to pull them back into their original state. A vast array of matrix metalloproteases (MMPs) is also altered: MMP-1a and -7 are upregulated, while MMP-3, -13, -25 are downregulated. MMP-3 and -13 have previously been shown to positively correlate with the degree of obesity, while MMP-7 negatively correlates with the degree of obesity (11, 36).

The metabolic improvements coincide with a decrease in inflammation in adipose tissue. Obesity is characterized by a chronic inflammatory state, during which macrophages are recruited into adipose tissue to enhance the local inflammatory program. The mechanisms of macrophage recruitment are complex, with numerous chemokines and cytokines implicated in the process (54, 56). Obesity is further accompanied by adipocyte expansion, which increases the likelihood that the disproportionately large adipocytes will undergo necrotic cell death, which can further potentiate local inflammation. Improvements in metabolism can also reverse this obesity-associated inflammatory phenotype, and vice versa (28). Since the *col6KOob/ob* mice have shown various metabolic improvements, we addressed the possible effects on inflammation by examining macrophage infiltration in these mice. Epididymal adipose tissue sections were stained for F4/80, a macrophage-specific cell surface marker. These histological stains hinted at a reduced macrophage infiltration in *col6KOob/ob* mice relative to *ob/ob* mice, although this was difficult to determine by visual inspection (Fig. 6A). This was supported by a more quantitative assessment by qRT-PCR analysis of F4/80 mRNA levels, which showed trends toward reduced levels of this macrophage marker in epididymal and significantly reduced levels in mesenteric fat (Fig. 6B). This decrease in local inflammation was also supported by analysis of other inflammatory genes. MCP-1 and SAA-3 mRNA levels were significantly decreased in mesenteric fat, while there was a trend toward reduced levels in epididymal fat. From this, it is apparent that mesenteric fat is more responsive to reduced levels of proinflammatory markers than epididymal fat (Fig. 6B). In line with a possible anti-inflammatory role of PPARγ in collagen VI-null adipose tissue, PPARγ mRNA levels are increased in mesenteric fat from *col6KOob/ob* mice (Fig. 6C).

One possible explanation for the generalized phenomenon in which large adipocytes typically suffer high-grade inflammation is that the large lipid droplet within an adipocyte exerts a substantial amount of pressure on the plasma membrane in its attempt to further expand. However, since adipocytes are usually constrained in a very rigid extracellular matrix environment, the strain on the adipocyte membrane from the expanding lipid droplet may trigger a significant degree of shear stress on the membrane. There are indisputably many phenomena
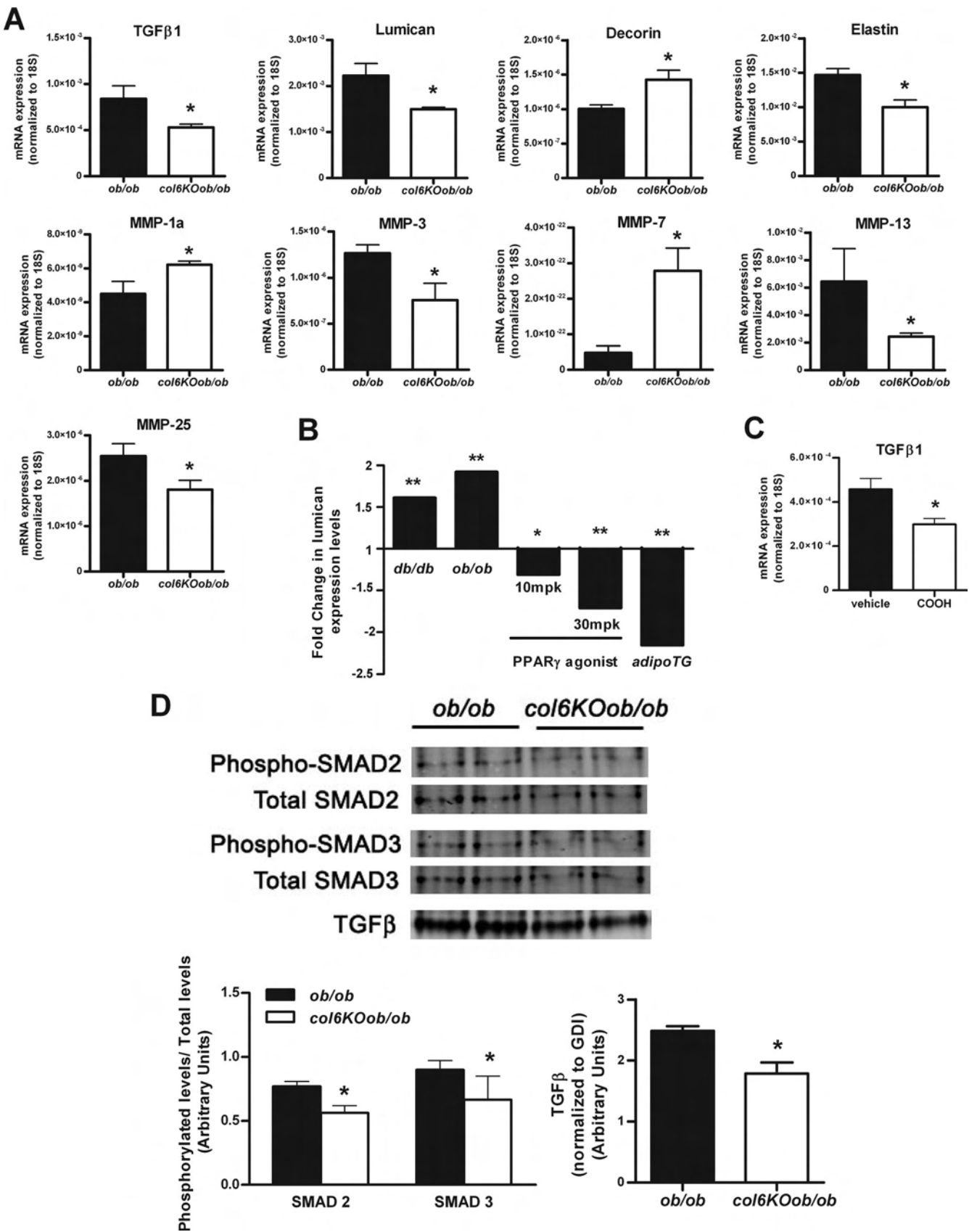
FIG. 5. *col6KOob/ob* mice have reduced TGF-β signaling. (A) Expression levels of extracellular matrix genes (TGF-β1, decorin, lumican, elastin, and several MMPs) were measured by qRT-PCR in epididymal fat from 8-week-old *col6KOob/ob* and *ob/ob* mice. Expression levels were

that can contribute to increased inflammation. We find that the activity of key regulatory kinases involved in shear stress, ERK and JNK, are significantly reduced in the *col6KOob/ob* adipocyte. These effects are pronounced for ERK and somewhat less dramatic for JNK, while p38 mitogen-activated protein kinase (MAPK) is unaffected. The reduced ERK activity is consistent with reduced shear stress on the *col6KOob/ob* membrane and supports the concept that a more flexible extracellular matrix environment can enable adipocytes to expand freely without the constraints of a rigid extracellular environment (Fig. 6D).

Collagen VI-null mice have reduced inflammation in response to an endotoxin challenge. We have previously shown that adipose tissue can make significant contributions to systemic inflammation, even in the context of potent proinflammatory stimuli such as endotoxin. An elevated baseline inflammatory level in adipose tissue that is already primed by a constitutively elevated infiltration of macrophages tends to respond with a higher amplitude of inflammation upon a further systemic proinflammatory stimulus. We therefore examined whether the reduced baseline inflammatory level in *col6KO* mice translates to a reduced response upon endotoxin exposure (Fig. 6E). Circulating IL-6 and MCP-1 levels were in fact lower in *col6KO* mice 6 h post-LPS challenge (Fig. 6E, upper panel). This was further reflected with respect to induction of proinflammatory genes in adipose tissue under these conditions by cytokines, such as IL-6 and tumor necrosis factor alpha, which were significantly reduced after 90 min of endotoxin exposure (Fig. 6E, lower panel).

Adipocytes from *col6KOob/ob* mice show reduced necrotic cell death. Obese fat is characterized by "crown-like structures" (CLS), which consist of necrotic adipocytes surrounded by activated macrophages. The degree of adipocyte necrosis has been demonstrated to positively correlate with increased adipocyte cell size in obesity (13). However, based on immunohistochemistry, inflammatory gene profiling, and reduced MAP kinase activity, it is apparent that adipose tissue from the *col6KOob/ob* mice does not follow these conventional rules. In order to assess whether reduced extracellular rigidity associated with the *col6KOob/ob* adipocyte phenotype translates into a reduced level of adipocyte necrosis, we examined the distribution of crown-like structures in epididymal fat. Consistent with the presumed improved survival rate of large adipocytes, *col6KOob/ob* mice displayed a reduced number of CLS (Fig. 6F). This was confirmed by TUNEL staining of adipose tissue sections, revealing a reduced degree of cell death in the *col6KOob/ob* adipocytes (Fig. 6G). Therefore, it is likely that the larger adipocytes in the *col6KOob/ob* mice are able to expand due to the reduced constraints of the normally rigid extracellular matrix. This then has a positive impact on their survival rate, which further translates into a decrease in inflammation.

The reduced constraints are also apparent when looking at other stress markers. One such marker is Xbp1, which is a measurement gauge for stress in the endoplasmic reticulum. It is found in its constitutive form under normal conditions, whereas during stress, it is alternatively spliced and migrates to the nucleus. *col6KOob/ob* mice display a highly significant reduction of the spliced Xbp1s form compared to age-matched *ob/ob* littermates, reflecting a reduced level of cellular stress (Fig. 6H).

Metabolic differences induced by the absence of collagen VI. To test whether the absence of collagen VI could cause any fundamental differences in other metabolic parameters, we placed *col6KOob/ob* and *ob/ob* mice into metabolic chambers. We performed calorimetry measurements on mice that were older, a time when there are no longer significant differences in the rate of weight gain, absolute weight, or fat mass between *col6KOob/ob* and *ob/ob* mice. There was however a highly significant difference in food intake, with the *col6KOob/ob* mice consuming only half of the amount of food that *ob/ob* mice consumed despite comparable body weights and compositions at that stage (Fig. 7A). This can only in part be explained by the small but significant reduction in locomotion (Fig. 7B), particularly during the daytime. This was also reflected in the reduced oxygen consumption (VO_2) during the same time frame, which is a reflection of reduced energy expenditure during the daytime (Fig. 7C). In addition, the *col6KOob/ob* mice had an altered respiratory exchange ratio (RER), which is indicative of differential substrate utilization. The respiratory exchange ratio indicates whether lipids (RER, 0.7) or carbohydrates (RER, 1) are being preferentially oxidized. The RER of *col6KOob/ob* mice is significantly reduced throughout the entire light/dark cycle, indicating that they preferentially burn fatty acids, as opposed to *ob/ob* mice, which rely more on carbohydrates (Fig. 7D). This preference for fatty acid utilization in *col6KOob/ob* mice is similar to standard RER levels in lean mice and is also the predicted outcome of an increase in insulin sensitivity, such as that observed in the *col6KOob/ob* mice. Combined, these experiments reveal highly significant changes at the level of food intake and energy expenditure, with an overall trend toward a higher rate of fatty acid consumption.

DISCUSSION

Under normal circumstances, adipose tissue is considered a connective tissue of low density and high plasticity. However, here we have demonstrated that during progression to an obese state, the connective fiber content of adipose tissue increases dramatically, due to an upregulation of several collagens. As the collagen content increases, the overall rigidity of adipose tissue also increases, likely contributing to an increase

---

normalized to 18S rRNA. (B) Lumican expression levels correlate to various metabolic states. Expression levels were determined as described for Fig. 1D and are represented as the fold change. (C) TGF-β1 levels in epididymal adipose tissue from 10-week-old mice treated with 30 mg/kg COOH or vehicle for 14 days. Expression levels were measured by qRT-PCR and were normalized to 18S rRNA. (D) Western blot analysis of TGF-β and the phosphorylation state of TGF-β signaling mediators SMAD2 and SMAD3 in epididymal adipose tissue. Band intensities were quantitated with the LI-COR imaging system (LI-COR Biosciences) and are shown in the lower panel. For panels A to D, data are represented as means ± standard errors (*n* = four mice/group). *, $P < 0.05$; **, $P < 0.01$ (by Student's *t* test).
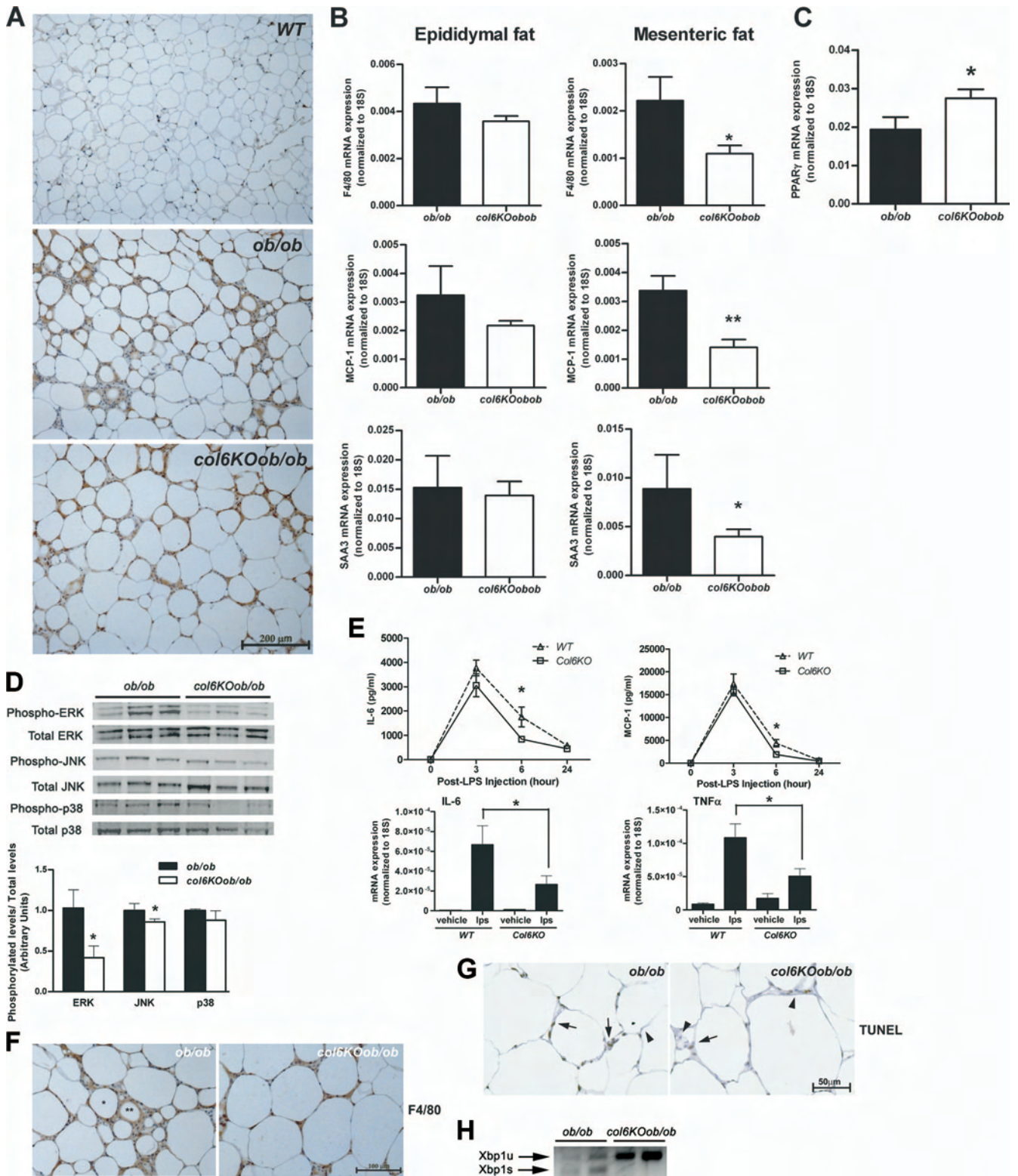
FIG. 6. Absence of collagen VI reduces systemic and adipose tissue-specific inflammation. (A) F4/80 immunohistochemical analysis of epididymal fat tissue sections from *col6KOob/ob* and *ob/ob* mice, as an indicator of the degree of macrophage infiltration of the tissue. (B) Quantitative real-time PCR analysis for the inflammatory cytokines F4/80, MCP-1, and SAA3 in epididymal and mesenteric fat. Expression levels of all genes were normalized to 18S rRNA (means ± standard errors; *n* = four mice/group). (C) qRT-PCR analysis of PPAR-γ expression in mesenteric fat. Expression levels were normalized to 18S rRNA (means ± standard errors; *n* = four mice/group). (D) Phosphorylation states of ERK, JNK, and p38 MAPK in epididymal adipose tissue from *col6KOob/ob* and *ob/ob* mice were determined by Western blotting with specific antibodies for their phosphorylated forms and for total levels. Band intensities were quantitated (means ± standard errors; *n* = three mice/group).
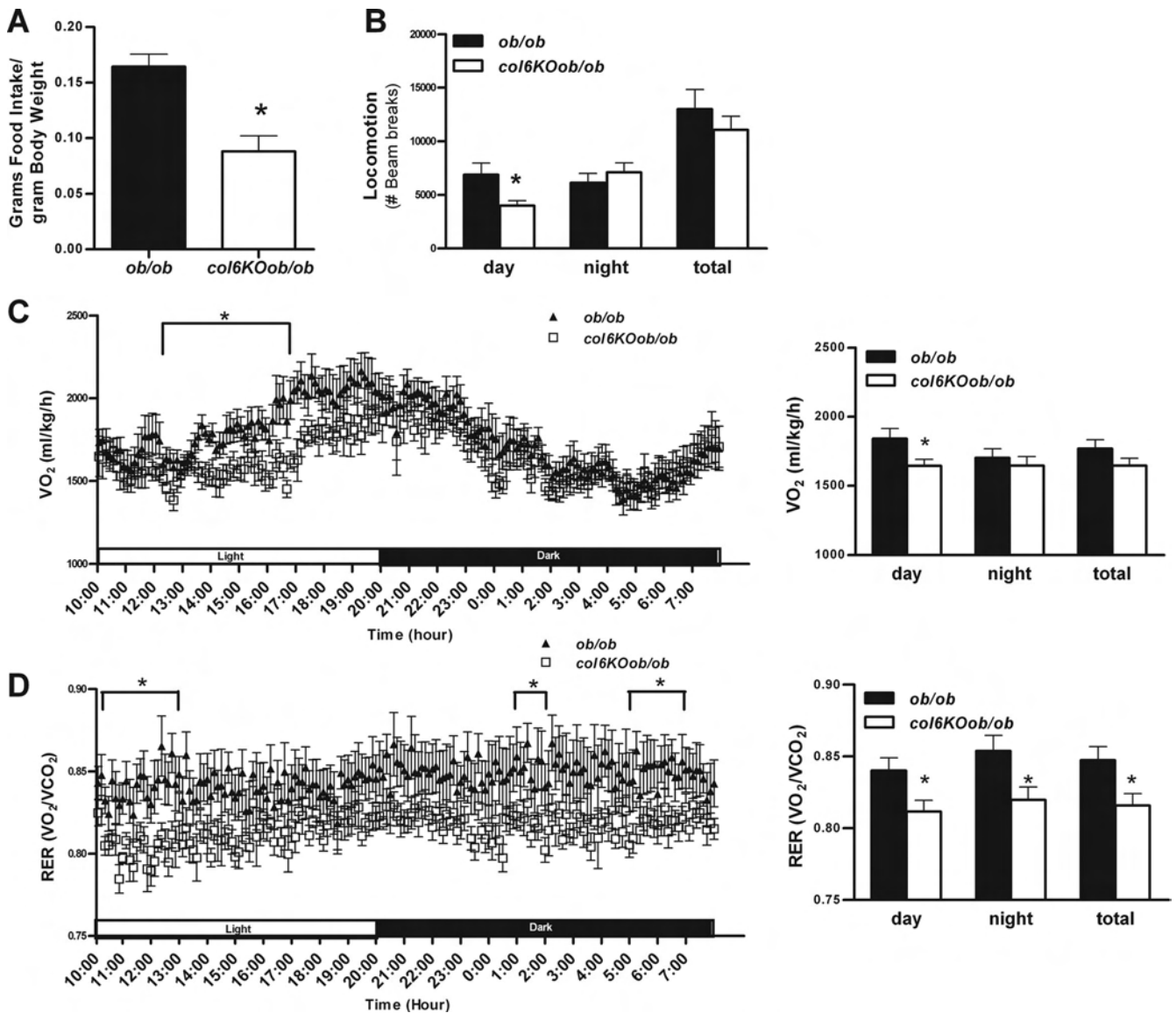
FIG. 7. Metabolic cage studies of *col6KOob/ob* mice and their *ob/ob* littermates. (A) Food intake was measured and is expressed as food intake/gram of body weight (means ± standard errors; *n* = four mice/group). (B to D) Total locomotion (ambulatory and rearing) (B), oxygen consumption (VO_2) (C), and RERs (D) were measured during the course of the day (means ± standard errors; *n* = four mice/group). All mice used in this experiment were 12 weeks old. *, $P < 0.05$ by Student's *t* test or two-way ANOVA.

in its mechanical strength. The term fibrosis has been defined as the formation of fibrous tissue as a reparative or reactive process; it has been widely utilized in the context of the liver, lung, and kidney, in addition to several other tissues. In adipose tissue, fibrosis appears to be initiated in response to adipocyte hypertrophy, which occurs as the initial step toward fat pad expansion through enlargement of the lipid droplet size in existing adipocytes. This cellular expansion seems to consti-

(E) LPS challenge in collagen VI-null and WT mice was performed. Circulating IL-6 and MCP-1 levels were measured (upper panel). mRNA expression levels of inflammatory cytokines IL-6 and tumor necrosis factor alpha (TNFα) was measured in epididymal fat by qRT-PCR and normalized to 18S rRNA 90 min after injection of LPS (lower panel) (means ± standard errors; *n* = four mice/group). (F) CLS were visualized in F4/80-stained epididymal adipose tissue sections. The single asterisk marks a representative CLS, while the double asterisk indicates a remnant lipid droplet after cell death. (G) Apoptotic adipocytes were visualized by TUNEL staining of epididymal tissue sections of *col6KOob/ob* and *ob/ob* mice. Brown staining is indicative of a TUNEL-positive nucleus (arrow), while blue staining (hematoxylin stain) represents a nonreactive nucleus (arrowhead). (H) Endoplasmic reticulum stress was measured by PCR analysis for Xbp-1. Primers spanning the splice junction were used to amplify unspliced and spliced forms of Xbp-1 and were separate on a 3% agarose gel. Unspliced Xbp-1 (Xbp1u) is 171 bp, while the spliced Xbp-1 (Xbp1s) is 145 bp and is a positive indication of endoplasmic reticulum stress. All experiments in this figure were performed with 10-week-old *col6KOob/ob* and *ob/ob* mice. *, $P < 0.05$ (data in panels B, C, D, and F were analyzed by Student's *t* test; data in panel E were analyzed by two-way ANOVA).

tute the initial "insult," in response to which the upregulation of extracellular matrix components is triggered. We are currently investigating which cellular factors couple the cellular expansion of the adipocyte with increased transcriptional activity at the level of collagens; our preliminary data suggest that hypoxia-inducible factor 1α plays a critical role in this process (N. Halberg et al., submitted for publication).

The level of extracellular matrix constituents in all tissues is a reflection of the balance between the rate of synthesis of matrix proteins and their degradation. Degradation is achieved through a family of proteins termed MMPs, which in turn are regulated by their inhibitors, called tissue inhibitors of MMPs. During tissue remodeling, the balance between these molecules can shift to accommodate the tissue's immediate needs for expansion. The altered expression of the proteoglycans lumican and decorin in *col6KOob/ob* mice has fundamental implications in the antifibrotic nature of the fat.

Lumican has been implicated in various processes, such as cell migration, proliferation, wound healing, and inflammation. One of its more unique roles is its ability to bind and interact with macrophages, an interaction for which its keratan sulfate side chains are critical (19). Decorin is well-known for its antifibrotic role in lung, kidney, muscle, and liver through its ability to inhibit TGF-β (25, 27, 30). TGF-β, in turn, plays a central role in modulating the balance between the rate of synthesis and degradation of matrix proteins. TGF-β contributes to fibrosis of several tissues: by increasing expression of matrix components, such as collagens, fibronectin, and matrix proteolgycans, and by inducing inhibitors of matrix-degrading MMPs. Therefore, despite the fact that lumican and decorin are both collagen cross-linking proteins, these two proteins have opposing roles in fibrosis. This could be due to their specific roles during collagen fibrillogenesis or due to the diverse interactions that their unique proteoglycan side chains enable (19, 40). The downregulation of lumican and TGF-β and the upregulation of decorin suggest a mechanism of reduced fat fibrosis in collagen VI-deficient *ob/ob* mice.

Recent reports have described a role for PPARγ as a potent antifibrotic factor. PPARγ agonists can reduce fibrosis in several organs, including kidneys, liver, heart, and lungs (1, 42, 43, 58). It has been suggested that the PPARγ agonist tesaglitazar, a member of the thiazolidinedione (TZD) family, reduces glomerulofibrosis and collagen deposition by lowering TGF-β1 levels in the kidney (8). Xu and colleagues have demonstrated that PPARγ can act as a repressor of type I collagen synthesis by increasing gamma interferon-induced repression of collagen synthesis (57). We have demonstrated here that COOH, a selective non-TZD-based PPARγ agonist, reduces the expression levels of a vast majority of collagens in adipose tissue. This provides an alternative mechanism of action, by which TZDs can improve the diabetic phenotype through the lowering of the overall extracellular matrix content of adipose tissue.

Since TGF-β1 plays a critical role in collagen deposition, it is likely a target of PPARγ agonist-induced reductions in collagen levels. In fact, we found that wild-type mice treated with a PPARγ agonist have reduced levels of TGF-β1 in adipose tissue (Fig. 5C). The reduction of TGF-β1 levels in *col6 KOob/ob* mice is consistent with a possible role of TGF-β in inducing fibrosis of adipose tissue as well. TGF-β can also be upregulated by mechanical stress in many cell types (6, 29, 34,

49, 53). Mechanical stress on the adipocyte membrane, triggered by the expanding lipid droplet, may also be the source of shear stress at the level of the plasma membrane. Similar to what has been reported for many other tissues in response to mechanical stress, TGF-β is likely to upregulate collagens and other extracellular matrix proteins to counteract this expansion. During times of positive energy balance, there is, however, continued pressure on the adipocyte to expand further. The increased rigidity of the adipose tissue matrix counteracts this trend for further expansion. Such a tug-of-war between cellular expansion of adipocytes and the rigid extracellular environment exerts massive pressure on the plasma membrane that can result in cell death by necrosis. Demeulemeester and colleagues demonstrated that mice treated with an MMP inhibitor while receiving a high-fat diet challenge had less adipose tissue, increased adipocyte cell number, and decreased average adipocyte diameter. Their increased adipose collagen content coupled with reduced adipocyte size is consistent with the notion that increased collagen restricts expansion of adipocytes (17). A reduced level of elastin in *col6KOob/ob* adipose tissue is also consistent with a more flexible microenvironment of the adipocyte.

One major characteristic of obese adipose tissue is an increased frequency of adipocyte cell death. Work by Cinti et al. demonstrated that macrophages aggregate around these dead adipocytes and become increasingly activated in their attempt to clear the potentially cytotoxic remnant lipid droplet (13). These adipose tissue macrophages fuse to form multinucleated cells and surround each dead adipocyte in a crown-like structure. In addition to this phenomenon, the number of necrotic adipocytes positively correlates with average adipocyte size in obese mice and other mouse models of adipocyte hypertrophy (13, 50). Hormone-sensitive lipase (HSL) knockout mice exhibit adipocyte hypertrophy and macrophage recruitment without any other characteristics of obesity. However, since HSL-deficient mice possess the typical rigid environment, in contrast to our *col6KOob/ob* mice, it is likely that adipocytes in HSL-deficient mice encounter increased shear stress, cell death, and inflammation.

Shear stress and membrane stretching have been shown to activate members of the MAPK family in several cell types (23, 32, 44, 51). In response to shear stress, large adipocytes exhibit an increased level of activation of the β1-integrin/ERK signaling pathway (18). In some circumstances, mechanical stretching-induced activation of JNK can also result in apoptosis of cells (41). Therefore, shear stress in large adipocytes appears to be the trigger for adipocyte death and the impending inflammation. The association of adipocyte hypertrophy with increased macrophage recruitment has led to the current dogma that an increase in adipocyte size is indicative of inflamed adipose tissue and is generally associated with an unfavorable metabolic profile. In contrast, in the absence of collagen VI, the adipocyte matrix has more flexibility and allows adipocytes to continue to expand without the associated necrosis and inflammation. This may be one of the reasons why the *col6KOob/ob* mice defy the currently established rule that larger adipocytes are associated with increased inflammation.

Since an array of signaling molecules, including many upstream regulators of ERK and JNK, reside in caveolae, it has

been suggested that shear stress-induced MAPK activation involves caveolae (5, 44). Park and colleagues demonstrated that exposure of endothelial cells to shear stress dramatically increases the number of invaginated caveolae. *ob/ob* mice deficient in collagen VI have an accumulation of uninvaginated, vesicular caveolae in their adipocytes. The differences in caveolar structures between the *col6KOob/ob* and *ob/ob* mice are therefore a direct reflection of the reduced levels of shear stress in the *col6KOob/ob* mice.

The data presented here are consistent with the concept that reduced local inflammation in the adipose tissue of *col6KOob/ob* mice is the major contributing factor to their overall improvement in the metabolic phenotype. The weakened extracellular matrix environment in *col6KOob/ob* adipose tissue enables their adipocytes to expand unhindered, thus facilitating storage of excess lipids and reducing ectopic lipid deposition. *col6KOob/ob* mice also become more insulin sensitive, as depicted in their reduced islet hyperplasia and improvements in overall islet morphology.

The extracellular matrix is extremely important for structure and function of almost any cell type; furthermore, it is involved in numerous processes such as cell adhesion, proliferation, differentiation, migration, apoptosis, and gene induction (20). In adipose tissue, it is particularly crucial for maintaining structural integrity of adipocytes and plays a critical role in adipogenesis. There are specific sequential alterations in the extracellular milieu during adipocyte differentiation, with a cascade of activation and deactivation of various MMPs, complementing the creation and destruction of the collagen network (31, 33). Treatment of 3T3-L1 preadipocytes with a broad-specificity MMP inhibitor hinders the formation of fully differentiated lipid-laden adipocytes (11, 16). The extracellular matrix also undergoes numerous changes during obesity, with the MMP/tissue inhibitors of MMP balance being shifted toward increased matrix degradation, presumably as a compensatory response to the increased collagen content during obesity (11, 17). Despite the clear relevance of the matrix on adipocytes, very few studies have focused on a thorough characterization of the metabolic impact of the extracellular matrix during obesity or during other metabolic conditions.

One of the first available examples of a metabolic study devoted to an extracellular matrix protein in adipose tissue was a study on SPARC, a matricellular protein involved in cell-extracellular matrix interactions. SPARC-null mice have a larger epididymal fat pad and an increased number of adipocytes in skin. Even though we lack information on any metabolic consequences that the absence of SPARC causes, this was the first time that an extracellular matrix protein was implicated in an effect on adipose tissue. More recently, Chun and colleagues demonstrated that the absence of matrix metalloproteinase MT1-MMP causes lipodystrophy in mice by impairing white adipose tissue development, due to a direct impact of MT1-MMP on adipocyte differentiation (12). Interestingly, these effects could only be observed in vitro, when cells were grown in a three-dimensional matrix.

We selected collagen VI as a candidate matrix component and studied its impact on adipose tissue physiology. Collagen VI is an ideal candidate due to its relatively abundant and highly enriched expression in adipose tissue. It is the most highly expressed collagen in differentiated adipocytes and undergoes dramatic structural changes during adipogenesis (38). Collagen VI fibrils alter their appearance during differentiation of 3T3-L1 preadipocytes, switching from a thin fibril texture at day 4 of differentiation to a very thick appearance in fully differentiated adipocytes. Several studies have further demonstrated that collagen VI levels correlate with conditions of hyperglycemia and insulin resistance (2, 37). We have previously demonstrated a role for adipocyte-derived collagen VI in progression of mammary tumor growth (26). During tumor growth, a proteolytic cleavage event occurs and the resulting C-terminal collagen VI fragments accumulate in tumor cells, activating the NG2 receptor and promoting a mitogenic response in the cancer cells. Our data describing increased mammary epithelial apoptosis in the absence of collagen VI protein are compatible with previous data that have demonstrated the requirement of collagen VI in the prevention of apoptosis and its stimulatory role in proliferation through AKT signaling events (22). The absence of collagen VI results in a proapoptotic signal event, thus reducing the likelihood of tumor proliferation.

Our observations have highlighted a number of changes at the level of food intake and energy expenditure: the lack of collagen VI triggers reduced food intake and reduced energy expenditure, with a higher rate of fatty acid consumption. Since these changes are not only observed during high fat diet exposure but also in the *ob/ob* background, these phenomena cannot exclusively be driven by leptin. It is not clear how the reported changes in adipose tissue trigger the systemic alterations in food intake and energy expenditure. These are questions of obvious interest that we are currently pursuing. In addition, we cannot formally rule out that collagen VI exerts its impact on metabolic control through action in tissues other than fat.

In summary, our study highlights the fact that collagen VI, and possibly additional extracellular matrix constituents, are extremely important in modulating adipocyte physiology. Collagen VI has an essential role in the fibrotic component of obesity and directly affects the ability of adipocytes to expand. The involvement of collagen VI in obesity opens a new chapter in which the adipocyte itself affects overall metabolic function; however, it is now apparent that the extracellular matrix environment surrounding the adipocyte can also play an essential role. Further studies will be required to explore the physiological consequences of adipose tissue fibrosis and whether collagen VI plays a critical role in other fibrotic tissues.

REFERENCES

1. **Belvisi, M. G., D. J. Hele, and M. A. Birrell.** 2006. Peroxisome proliferator-activated receptor gamma agonists as therapy for chronic airway inflammation. Eur. J. Pharmacol. **533:**101–109.
2. **Berria, R., L. Wang, D. K. Richardson, J. Finlayson, R. Belfort, T. Pratipanawatr, E. A. De Filippis, S. Kashyap, and L. J. Mandarino.** 2006. Increased collagen content in insulin-resistant skeletal muscle. Am. J. Physiol. Endocrinol. Metab. **290:**E560–E565.
3. **Bidanset, D. J., C. Guidry, L. C. Rosenberg, H. U. Choi, R. Timpl, and M. Hook.** 1992. Binding of the proteoglycan decorin to collagen type VI. J. Biol. Chem. **267:**5250–5256.
4. **Bonaldo, P., P. Braghetta, M. Zanetti, S. Piccolo, D. Volpin, and G. M. Bressan.** 1998. Collagen VI deficiency induces early onset myopathy in the mouse: an animal model for Bethlem myopathy. Hum. Mol. Genet. **7:**2135–2140.
5. **Boyd, N. L., H. Park, H. Yi, Y. C. Boo, G. P. Sorescu, M. Sykes, and H. Jo.** 2003. Chronic shear induces caveolae formation and alters ERK and Akt responses in endothelial cells. Am. J. Physiol. Heart Circ. Physiol. **285:**H1113–H1122.
6. **Branton, M. H., and J. B. Kopp.** 1999. TGF-beta and fibrosis. Microbes Infect. **1:**1349–1365.
6a.**Carr, T. P., C. J. Andresen, and L. L. Rudel.** 1993. Enzymatic determination of triglyceride, free cholesterol, and total cholesterol in tissue lipid extracts. Clin. Biochem. **26:**39–42.
7. **Cederberg, A., L. M. Gronning, B. Ahren, K. Tasken, P. Carlsson, and S. Enerback.** 2001. FOXC2 is a winged helix gene that counteracts obesity, hypertriglyceridemia, and diet-induced insulin resistance. Cell **106:**563–573.
8. **Cha, D. R., X. Zhang, Y. Zhang, J. Wu, D. Su, J. Y. Han, X. Fang, B. Yu, M. D. Breyer, and Y. Guan.** 2007. Peroxisome proliferator activated receptor alpha/gamma dual agonist tesaglitazar attenuates diabetic nephropathy in db/db mice. Diabetes **56:**2036–2045.
9. **Chandalia, M., A. V. Cabo-Chan, Jr., S. Devaraj, I. Jialal, S. M. Grundy, and N. Abate.** 2003. Elevated plasma high-sensitivity C-reactive protein concentrations in Asian Indians living in the United States. J. Clin. Endocrinol. Metab. **88:**3773–3776.
10. **Chandalia, M., P. Lin, T. Seenivasan, E. H. Livingston, P. G. Snell, S. M. Grundy, and N. Abate.** 2007. Insulin resistance and body fat distribution in South Asian men compared to Caucasian men. PLoS ONE **2:**e812.
11. **Chavey, C., B. Mari, M. N. Monthouel, S. Bonnafous, P. Anglard, E. Van Obberghen, and S. Tartare-Deckert.** 2003. Matrix metalloproteinases are differentially expressed in adipose tissue during obesity and modulate adipocyte differentiation. J. Biol. Chem. **278:**11888–11896.
12. **Chun, T. H., K. B. Hotary, F. Sabeh, A. R. Saltiel, E. D. Allen, and S. J. Weiss.** 2006. A pericellular collagenase directs the 3-dimensional development of white adipose tissue. Cell **125:**577–591.
13. **Cinti, S., G. Mitchell, G. Barbatelli, I. Murano, E. Ceresi, E. Faloia, S. Wang, M. Fortier, A. S. Greenberg, and M. S. Obin.** 2005. Adipocyte death defines macrophage localization and function in adipose tissue of obese mice and humans. J. Lipid Res. **46:**2347–2355.
14. **Cohen, A. W., B. Razani, X. B. Wang, T. P. Combs, T. M. Williams, P. E. Scherer, and M. P. Lisanti.** 2003. Caveolin-1-deficient mice show insulin resistance and defective insulin receptor protein expression in adipose tissue. Am. J. Physiol. Cell Physiol. **285:**C222–C235.
15. **Combs, T. P., U. B. Pajvani, A. H. Berg, Y. Lin, L. A. Jelicks, M. Laplante, A. R. Nawrocki, M. W. Rajala, A. F. Parlow, L. Cheeseboro, Y. Y. Ding, R. G. Russell, D. Lindemann, A. Hartley, G. R. Baker, S. Obici, Y. Deshaies, M. Ludgate, L. Rossetti, and P. E. Scherer.** 2004. A transgenic mouse with a deletion in the collagenous domain of adiponectin displays elevated circulating adiponectin and improved insulin sensitivity. Endocrinology **145:**367–383.
16. **Croissandeau, G., M. Chretien, and M. Mbikay.** 2002. Involvement of matrix metalloproteinases in the adipose conversion of 3T3-L1 preadipocytes. Biochem. J. **364:**739–746.
17. **Demeulemeester, D., D. Collen, and H. R. Lijnen.** 2005. Effect of matrix metalloproteinase inhibition on adipose tissue development. Biochem. Biophys. Res. Commun. **329:**105–110.
18. **Farnier, C., S. Krief, M. Blache, F. Diot-Dupuy, G. Mory, P. Ferre, and R. Bazin.** 2003. Adipocyte functions are modulated by cell size change: potential involvement of an integrin/ERK signalling pathway. Int. J. Obes. Relat. Metab. Disord. **27:**1178–1186.
19. **Funderburgh, J. L., R. R. Mitschler, M. L. Funderburgh, M. R. Roth, S. K. Chapes, and G. W. Conrad.** 1997. Macrophage receptors for lumican. A corneal keratan sulfate proteoglycan. Investig. Ophthalmol. Vis. Sci. **38:**1159–1167.
20. **Hammar, E. B., J. C. Irminger, K. Rickenbach, G. Parnaud, P. Ribaux, D. Bosco, D. G. Rouiller, and P. A. Halban.** 2005. Activation of NF-κB by extracellular matrix is involved in spreading and glucose-stimulated insulin secretion of pancreatic beta cells. J. Biol. Chem. **280:**30630–30637.
21. **Hedbom, E., and D. Heinegard.** 1993. Binding of fibromodulin and decorin to separate sites on fibrillar collagens. J. Biol. Chem. **268:**27307–27312.
22. **Howell, S. J., and K. J. Doane.** 1998. Type VI collagen increases cell survival and prevents anti-beta 1 integrin-mediated apoptosis. Exp. Cell. Res. **241:**230–241.
23. **Hu, Y., B. W. Hochleitner, G. Wick, and Q. Xu.** 1998. Decline of shear stress-induced activation of extracellular signal-regulated kinases, but not stress-activated protein kinases, in in vitro propagated endothelial cells. Exp. Gerontol. **33:**601–613.
24. **Hughes, T. R., M. Mao, A. R. Jones, J. Burchard, M. J. Marton, K. W. Shannon, S. M. Lefkowitz, M. Ziman, J. M. Schelter, M. R. Meyer, S. Kobayashi, C. Davis, H. Dai, Y. D. He, S. B. Stephaniants, G. Cavet, W. L. Walker, A. West, E. Coffey, D. D. Shoemaker, R. Stoughton, A. P. Blanchard, S. H. Friend, and P. S. Linsley.** 2001. Expression profiling using microarrays fabricated by an ink-jet oligonucleotide synthesizer. Nat. Biotechnol. **19:**342–347.
25. **Isaka, Y., D. K. Brees, K. Ikegaya, Y. Kaneda, E. Imai, N. A. Noble, and W. A. Border.** 1996. Gene therapy by skeletal muscle expression of decorin prevents fibrotic disease in rat kidney. Nat. Med. **2:**418–423.
26. **Iyengar, P., V. Espina, T. W. Williams, Y. Lin, D. Berry, L. A. Jelicks, H. Lee, K. Temple, R. Graves, J. Pollard, N. Chopra, R. G. Russell, R. Sasisekharan, B. J. Trock, M. Lippman, V. S. Calvert, E. F. Petricoin III, L. Liotta, E. Dadachova, R. G. Pestell, M. P. Lisanti, P. Bonaldo, and P. E. Scherer.** 2005. Adipocyte-derived collagen VI affects early mammary tumor progression in vivo, demonstrating a critical interaction in the tumor/stroma microenvironment. J. Clin. Investig. **115:**1163–1176.
27. **Kanzler, S., A. W. Lohse, A. Keil, J. Henninger, H. P. Dienes, P. Schirmacher, S. Rose-John, K. H. zum Buschenfelde, and M. Blessing.** 1999. TGF-β1 in liver fibrosis: an inducible transgenic mouse model to study liver fibrogenesis. Am. J. Physiol. **276:**G1059–G1068.
28. **Kim, J. Y., E. van de Wall, M. Laplante, A. Azzara, M. E. Trujillo, S. M. Hofmann, T. Schraw, J. L. Durand, H. Li, G. Li, L. A. Jelicks, M. F. Mehler, D. Y. Hui, Y. Deshaies, G. I. Shulman, G. J. Schwartz, and P. E. Scherer.** 2007. Obesity-associated improvements in metabolic profile through expansion of adipose tissue. J. Clin. Investig. **117:**2621–2637.
29. **Klein-Nulend, J., M. H. Helfrich, J. G. Sterck, H. MacPherson, M. Joldersma, S. H. Ralston, C. M. Semeins, and E. H. Burger.** 1998. Nitric oxide response to shear stress by human bone cell cultures is endothelial nitric oxide synthase dependent. Biochem. Biophys. Res. Commun. **250:**108–114.
30. **Kolb, M., P. J. Margetts, P. J. Sime, and J. Gauldie.** 2001. Proteoglycans decorin and biglycan differentially modulate TGF-beta-mediated fibrotic responses in the lung. Am. J. Physiol. Lung Cell. Mol. Physiol. **280:**L1327–L1334.
31. **Kubo, Y., S. Kaidzu, I. Nakajima, K. Takenouchi, and F. Nakamura.** 2000. Organization of extracellular matrix components during differentiation of adipocytes in long-term culture. In Vitro Cell. Dev. Biol. Anim. **36:**38–44.
32. **Li, C., and Q. Xu.** 2000. Mechanical stress-initiated signal transductions in vascular smooth muscle cells. Cell. Signal. **12:**435–445.
33. **Lilla, J., D. Stickens, and Z. Werb.** 2002. Metalloproteases and adipogenesis: a weighty subject. Am. J. Pathol. **160:**1551–1554.
34. **Liton, P. B., X. Liu, P. Challa, D. L. Epstein, and P. Gonzalez.** 2005. Induction of TGF-β1 in the trabecular meshwork under cyclic mechanical stress. J. Cell. Physiol. **205:**364–371.
35. **Livak, K. J., and T. D. Schmittgen.** 2001. Analysis of relative gene expression data using real-time quantitative PCR and the 2(-ΔΔC_T) method. Methods **25:**402–408.
36. **Maquoi, E., C. Munaut, A. Colige, D. Collen, and H. R. Lijnen.** 2002. Modulation of adipose tissue expression of murine matrix metalloproteinases and their tissue inhibitors with obesity. Diabetes **51:**1093–1101.
37. **Muona, P., S. Jaakkola, R. Z. Zhang, T. C. Pan, L. Pelliniemi, L. Risteli, M. L. Chu, J. Uitto, and J. Peltonen.** 1993. Hyperglycemic glucose concentrations up-regulate the expression of type VI collagen in vitro. Relevance to alterations of peripheral nerves in diabetes mellitus. Am. J. Pathol. **142:**1586–1597.
38. **Nakajima, I., S. Muroya, R. Tanabe, and K. Chikuni.** 2002. Extracellular matrix development during differentiation into adipocytes with a unique increase in type V and VI collagen. Biol. Cell **94:**197–203.
39. **Nakajima, I., T. Yamaguchi, K. Ozutsumi, and H. Aso.** 1998. Adipose tissue extracellular matrix: newly organized by adipocytes during differentiation. Differentiation **63:**193–200.
40. **Neame, P. J., C. J. Kay, D. J. McQuillan, M. P. Beales, and J. R. Hassell.** 2000. Independent modulation of collagen fibrillogenesis by decorin and lumican. Cell. Mol. Life Sci. **57:**859–863.
41. **Nguyen, H. T., M. H. Hsieh, A. Gaborro, B. Tinloy, C. Phillips, and R. M. Adam.** 2006. JNK/SAPK and p38 SAPK-2 mediate mechanical stretch-induced apoptosis via caspase-3 and -9 in NRK-52E renal epithelial cells. Nephron. Exp. Nephrol. **102:**e49–e61.
42. **Ogata, T., T. Miyauchi, S. Sakai, M. Takanashi, Y. Irukayama-Tomobe, and I. Yamaguchi.** 2004. Myocardial fibrosis and diastolic dysfunction in deoxycorticosterone acetate-salt hypertensive rats is ameliorated by the peroxisome proliferator-activated receptor-alpha activator fenofibrate, partly by suppressing

inflammatory responses associated with the nuclear factor-kappa-B pathway. J. Am. Coll. Cardiol. **43:**1481–1488.

43. **Panchapakesan, U., S. Sumual, C. A. Pollock, and X. Chen.** 2005. PPARγ agonists exert antifibrotic effects in renal tubular cells exposed to high glucose. Am. J. Physiol. Renal Physiol. **289:**F1153–F1158.

44. **Park, H., Y. M. Go, P. L. St John, M. C. Maland, M. P. Lisanti, D. R. Abrahamson, and H. Jo.** 1998. Plasma membrane cholesterol is a key molecule in shear stress-dependent activation of extracellular signal-regulated kinase. J. Biol. Chem. **273:**32304–32311.

45. **Rada, J. A., P. K. Cornuet, and J. R. Hassell.** 1993. Regulation of corneal collagen fibrillogenesis in vitro by corneal proteoglycan (lumican and decorin) core proteins. Exp. Eye Res. **56:**635–648.

46. **Saika, S., T. Miyamoto, S. Tanaka, T. Tanaka, I. Ishida, Y. Ohnishi, A. Ooshima, T. Ishiwata, G. Asano, T. Chikama, A. Shiraishi, C. Y. Liu, C. W. Kao, and W. W. Kao.** 2003. Response of lens epithelial cells to injury: role of lumican in epithelial-mesenchymal transition. Investig. Ophthalmol. Vis. Sci. **44:**2094–2102.

47. **Sakuraba, H., H. Mizukami, N. Yagihashi, R. Wada, C. Hanyu, and S. Yagihashi.** 2002. Reduced beta-cell mass and expression of oxidative stress-related DNA damage in the islet of Japanese type II diabetic patients. Diabetologia **45:**85–96.

48. **Scherer, P. E., P. E. Bickel, M. Kotler, and H. F. Lodish.** 1998. Cloning of cell-specific secreted and surface proteins by subtractive antibody screening. Nat. Biotechnol. **16:**581–586.

49. **Sterck, J. G., J. Klein-Nulend, P. Lips, and E. H. Burger.** 1998. Response of normal and osteoporotic human bone cells to mechanical stress in vitro. Am. J. Physiol. **274:**E1113–E1120.

50. **Strissel, K. J., Z. Stancheva, H. Miyoshi, J. W. Perfield II, J. DeFuria, Z. Jick, A. S. Greenberg, and M. S. Obin.** 2007. Adipocyte death, adipose tissue remodeling, and obesity complications. Diabetes **56:**2910–2918.

51. **Sumpio, B. E., S. Yun, A. C. Cordova, M. Haga, J. Zhang, Y. Koh, and J. A. Madri.** 2005. MAPKs (ERK1/2, p38) and AKT can be phosphorylated by shear stress independently of platelet endothelial cell adhesion molecule-1 (CD31) in vascular endothelial cells. J. Biol. Chem. **280:**11185–11191.

52. **Takahashi, T., H. I. Cho, C. L. Kublin, and C. Cintron.** 1993. Keratan sulfate and dermatan sulfate proteoglycans associate with type VI collagen in fetal rabbit cornea. J. Histochem. Cytochem. **41:**1447–1457.

53. **Tschumperlin, D. J., J. D. Shively, T. Kikuchi, and J. M. Drazen.** 2003. Mechanical stress triggers selective release of fibrotic mediators from bronchial epithelium. Am. J. Respir. Cell Mol. Biol. **28:**142–149.

54. **Weisberg, S. P., D. McCann, M. Desai, M. Rosenbaum, R. L. Leibel, and A. W. Ferrante, Jr.** 2003. Obesity is associated with macrophage accumulation in adipose tissue. J. Clin. Investig. **112:**1796–1808.

55. **Woessner, J. F., Jr.** 1961. The determination of hydroxyproline in tissue and protein samples containing small proportions of this imino acid. Arch. Biochem. Biophys. **93:**440–447.

56. **Xu, H., G. T. Barnes, Q. Yang, G. Tan, D. Yang, C. J. Chou, J. Sole, A. Nichols, J. S. Ross, L. A. Tartaglia, and H. Chen.** 2003. Chronic inflammation in fat plays a crucial role in the development of obesity-related insulin resistance. J. Clin. Investig. **112:**1821–1830.

57. **Xu, Y., S. R. Farmer, and B. D. Smith.** 2007. Peroxisome proliferator-activated receptor gamma interacts with CIITA x RFX5 complex to repress type I collagen gene expression. J. Biol. Chem. **282:**26046–26056.

58. **Yang, L., C. C. Chan, O. S. Kwon, S. Liu, J. McGhee, S. A. Stimpson, L. Z. Chen, W. W. Harrington, W. T. Symonds, and D. C. Rockey.** 2006. Regulation of peroxisome proliferator-activated receptor-gamma in liver fibrosis. Am. J. Physiol. Gastrointest. Liver Physiol. **291:**G902–G911.